ROBUST AND OPTIMAL PID CONTROLLER SYNTHESIS FOR LINEAR TIME INVARIANT SYSTEMS

A Dissertation

by

SANGJIN HAN

Submitted to the Office of Graduate and Professional Studies of
Texas A&M University
in partial fulfillment of the requirements for the degree of

DOCTOR OF PHILOSOPHY

Chair of Committee,	Shankar P. Bhattacharyya
Committee Members,	Aniruddha Datta
	Raktim Bhattacharya
	Hamid Toliyat
Head of Department,	Miroslav Begovic

May 2019

Major Subject: Electrical Engineering

ABSTRACT

We dealt with new approaches to the design of Proportional-Integral-Derivative (PID) controllers and solved three important open problems: 1) Optimal design of H_∞ continuous time controllers 2) Optimal design of H_∞ discrete time controllers and 3) Design of PID controllers for prescribed settling time. We also deal with optimal Dynamic Compensator design for controllable and observable systems.

The main result of the first problem is a constructive determination of the set S_γ of stabilizing continuous PI and PID controllers achieving an H_∞ norm bound of γ on the error transfer function. This result utilizes the computation of the complete stabilizing set $\mathcal{S}$. We also point out connections between this H_∞ design and Gain and Phase Margin designs.

The main result of the second problem is a constructive characterization of the set $\mathcal{S}_\gamma$ of stabilizing digital controllers achieving a prescribed bound γ on the error transfer function. This is accomplished by utilizing the computation of $\mathcal{S}$, the set of all PID stabilizing controllers. The minimum achievable γ, denoted γ^* is also determined.

The main result of the third problem is a constructive determination of the set $\mathcal{S}(\sigma)$ of stabilizing PI and PID controllers with closed loop poles having real parts less than $-\sigma$. The signature method is applied to obtain the set $\mathcal{S}(\sigma)$ in the controller parameter space. The maximum achievable σ for a given plant is also determined.

The main result of the last problem is a new approach to design an optimal dynamic compensator. The system is augmented with a proper number of integrators and the state feedback of the augmented system is considered with a design parameter. The dynamic compensator is then designed such that the eigenvalues of the augmented system is identical to the closed loop spectrum of the implemented system with the compensator. By sweeping over the design parameter, multiple design specifications are compared within achievable boundary of performances.

DEDICATION

To my mother, my father, and my brother.

ACKNOWLEDGMENTS

Professor S. P. Bhattacharyya, my adviser, has taught, guided, supported and encouraged me over the last 5 years. He helped me to become an independent researcher who thinks critically and follows facts. I would like to express my deepest gratitude and respect to my adviser among all I have worked with so far.

I would like to extend my sincere appreciation to my committee members: Dr. A. Datta, Dr. R. Bhattacharya and Dr. H. Toliyat. They provided me with encouragement and patience throughout the prelim and final exam. I have discussed a number of fundamental topics with Dr. A. Datta inside and outside of his classes. Dr. R. Bhattacharya gave me interesting and meaningful questions to my dissertation. Dr. H. Toliyat helped me to have practical perspectives of my dissertation.

I would also extend my gratitude to Professor L. H. Keel and Professor W. Y. Joe from Tennessee State University. They encouraged me and expressed their sympathy by sharing their valuable thoughts and advices.

I had great pleasure of working with ESC team in ARL: Dr. William Nothwang, Dr. Joseph Conroy, Dr. E. Jared Shamwell, Paul Sabbagh, Nikolas Vale, Sarah Leung, Angela Maio, Dr. Justin Brody, Dr. Gregory Gremilion, Vinicious Goecks, Kyle Lindgren and Christopher Maxey,

I would like to express warm gratitude to my family. My mom, Youngsoon Byun, dad, Moonsoo Han, and brother, Sangbum Han, supported me in all directions. This dissertation is dedicated to them and their unconditional support.

I have met precious colleagues: Dr. D. N. Mohsenizadeh, Dr. I. D. Diaz Rodriguez. Their passion about the research and work enlightened and stimulated me. Special thanks to cool and awesome friends: Dr. Alejandro Yepes, Bharadwaj Satchidanandan, Byungjun Kim (Korean Navy Major), Cheng (Peter) Qian. Christian DeBuys, Hunter Williams, Hyun-Myung Woo, Janelle E. Morton, Jorge Ramos, John Buonocore, Kenny Chour, Kiyoeb Lee, Matthew Gardner, Miaomiao Zhao, Myung Seok Shim, Namita Anil Kumar, Niladri Das, Randy Kuhlmann, Salwan Sabry, Sanghoon Lee, Sunsoo Kim (Korean Air Force Major), Woorim Hong and Zhangxin Zhou.

CONTRIBUTORS AND FUNDING SOURCES

Contributors

This work was supervised by a dissertation committee consisting of Professor Shankar P. Bhattacharyya, Professor Aniruddha Datta, and Professor Hamid Toliyat of the Department of Electrical and Computer Engineering and Professor Raktim Bhattacharya of the Department of Aerospace Engineering.

All work for the dissertation was completed by the student, under the advisement of Professor Shankar P. Bhattacharyya of the Department of Electrical and Computer Engineering.

Funding Sources

There are no outside funding contributions to acknowledge related to the research and compilation of this document.

TABLE OF CONTENTS

Page

LIST OF FIGURES

FIGURE Page

1. INTRODUCTION

One of the central objective of controller design is to find controllers that bring both good stability margins and time performance characteristics in the feedback loop. For Proportional integral derivative (PID) controllers, we have the signature method that enables us to obtain a set of all stabilizing controllers, so called the stabilizing set. This dissertation deals with design methods of PID controllers that exploits the existence of the stabilizing set. For a given plant, having the stabilizing set in our hands opens to the challenge of multi-objective designs because in any design methodology, if there exists a PID controller satisfying an objective, then it must be a subset of the stabilizing set. Thus, in order to achieve multi-objective PID controller design, this dissertation focuses on the development of design specifications, calculated in terms of the controller gains, on the stabilizing set.

In this chapter, we introduce the stabilizing set and briefly summarize calculation procedures of the set using the concept of signature for continuous time systems and discrete time systems, separately.

In Chapter 2, we deal with the H_∞ norm of the error transfer function for continuous time plants. By superimposing the norm specification, the subset of the stabilizing set achieves robustness of the closed loop in terms of the H_∞ norm less than γ. In particular, the criterion for a fixed γ is equivalent to the outside of family of ellipses in the controller parameter space.

In Chapter 3, we extend this to the H_∞ norm of the error transfer function for discrete time plants. Since the majority of the controllers are implemented in practice by the digital controllers, we include several application examples.

In Chapter 4, we define σ-Hurwitz stability of a polynomial and apply this to find the subset of stabilizing set which renders the characteristic polynomial of the closed loop system has poles whose real part is less than $-\sigma$. Since the largest real part of the closed loop pole is related to the maximum decay of the system response, it developes a constructive determination of the subset of stabilizing set which achieves prescribed settling time specified the magnitude of σ. As we will

see, the subsets are telescoping as the prescribed σ values increases. Thus, we find the maximum achievable σ for a given plant when the stabilizing set shrinks gradually and just becomes empty.

In Chapter 5, we consider an arbitrary order controllers rather than fixed order controllers. Since the late 1950, the control field have started leaning towards state variable equations and time domain analysis using the equations. Doyle and Stein gave a counterexample to the almost perfect stability margin properties of Kalmans state feedback optimal control law and showed that if the controller was implemented using observer theory, such robust margins could vanish. We believe that this is majorly because of the separated steps for the optimal control law and the observer design. The optimality of the control law may only be valid when the order of the original system is not compromised by the compensators which are the realization of the estimates of unobservable states. Inspired by the earlier work of J. B. Pearson, we augment the system with a series of successive derivative of the input signals and make a use of the relationships among actual signals rather than virtual 'states'. Moreover, we give a systematic and simple approach to design an output feedback dynamic compensator such that we can compare mutiple design specifications such as gain and phase margins, H_∞ norms of the error transfer function and step responses, all of which will vary as the design parameter varies over the interval which guarantees the stability of the closed loop. We can fix the design parameter with which we obtain satisfactory specifications and moreover we can retrieve the controller from the fixed value of the design parameter.

In Chapter 6, we finish the dissertation with concluding remarks.

1.1 Signature Method for Continuous Time Systems

Consider a monic polynomial $\delta(s)$ of degree n with real coefficients. Let $\mathbb{C}^-$ denote the open left-half plane (LHP), $\mathbb{C}^+$ the closed right-half plane (RHP), and δ^- and δ^+ the numbers of roots of $\delta(s)$ in $\mathbb{C}^-$ and $\mathbb{C}^+$, respectively and assume that $\delta(s)$ has no $j\omega$ axis roots. Let $\angle\delta(j\omega)$ denote the phase of $\delta(s)$ at $s = j\omega$. The net change in the phase of $\delta(s)|_{s=j\omega}$ from $\omega = 0$ to $\omega = \infty$ is easily seen to be:

$$\Delta_{\omega=0}^{\infty}\angle\delta(j\omega) = \frac{\pi}{2}(\delta^- - \delta^+). \tag{1.1}$$

We call $\delta^- - \delta^+$ the Hurwitz *signature* of $\delta(s)$ and denote it as

$$\text{signature}(\delta) := \delta^- - \delta^+. \tag{1.2}$$

The signature of a polynomial $\delta(s)$ can be determined by knowing the zeros of the imaginary part of $\delta(j\omega)$ and the signs of the real part of $\delta(j\omega)$ at these zeros. In the following we describe how this can be exploited to determine the stabilizing set $\mathcal{S}$. Now consider a unity feedback loop with a PID controller and a plant in Fig. 1.1,

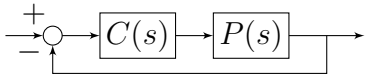

Figure 1.1: Unity feedback control loop.

where

$$P(s) = \frac{N(s)}{D(s)}, \;\; C(s) = k_p + \frac{k_i}{s} + k_d s, \tag{1.3}$$

and $D(s)$, $N(s)$ are polynomials of degree n and m, respectively, with real coefficients. We assume that $D(s)$ and $N(s)$ are coprime, that is, they have no common roots and $N(0) \neq 0$. The characteristic polynomial of the closed loop system is

$$\delta(s, k_p, k_i, k_d) = sD(s) + (k_i + k_p s + k_d s^2)N(s). \tag{1.4}$$

Define $\mathcal{S}$ to be the set of all stabilizing PID controllers:

$$\mathcal{S} := \{(k_p, k_i, k_d) \text{: } \delta(s, k_p, k_i, k_d) \text{ is Hurwitz}\}. \tag{1.5}$$

For stability, we must have

$$\text{signature}(\delta(s, k_p, k_i, k_d)) = n + 1, \;\; \forall (k_p, k_i, k_d) \in \mathcal{S}. \tag{1.6}$$

To achieve a separation of the gains into the real and imaginary parts, introduce the new polynomial

$$\nu(s) := \delta(s, k_p, k_i, k_d)N(-s). \tag{1.7}$$

Assume $N(s)$ has no roots on the imaginary axis. Let z^- and z^+ denote the numbers of roots of $N(s)$ in $\mathbb{C}^-$ and $\mathbb{C}^+$, respectively. Then $\delta(s)$ is Hurwitz stable if and only if

$$\begin{aligned} \text{signature}(\nu) &= n + 1 - z^- + z^+ \\ &= n + 1 - m + 2z^+. \end{aligned} \tag{1.8}$$

The stabilizing set $\mathcal{S}$ can now be described as

$$\mathcal{S} := \{(k_p, k_i, k_d)\text{: (1.8) is satisfied.}\}$$

In $\nu(s)$, k_p only appears in the odd degree terms of s while k_i and k_d only appear in the even degree terms of s. For a fixed $k_p = k_p^*$, there exist sets of linear inequalities in terms of k_i and k_d satisfying the signature condition in (1.8). The intersection of the inequalities for each set is thus convex in (k_i, k_d) space and the union of nonempty intersections is the stabilizing set for k_p^*. The procedure to find the entire set $\mathcal{S}$ is summarized in the following.

- Define $\nu_{even}(s^2)$ and $\nu_{odd}(s^2)$ such that

$$\nu(s) = \nu_{even}(s^2) + s\nu_{odd}(s^2).$$

- Fix $k_p = k_p^*$ and let $0 < \omega_1 < \omega_2 < \cdots < \omega_{l-1}$ denote the positive finite frequencies which are zeros of

$$\nu_{odd}(-\omega^2, k_p) = 0 \tag{1.9}$$

  of odd multiplicities. Let $\omega_0 := 0$ and $\omega_l := \infty$.

- Write $j = \text{sgn}[\nu_{odd}(0^+, k_p^*)]$ and determine the strings of integers i_0, i_1, ... such that

$$\begin{aligned} & n - m + 1 + 2z^+ \\ & = \begin{cases} j(i_0 + 2\sum_{t=1}^{l-1}(-1)^t i_t), & \text{if } n+m \text{ odd}, \\ j(i_0 + 2\sum_{t=1}^{l-1}(-1)^t i_t + (-1)^l i_l), & \text{if } n+m \text{ even}. \end{cases} \end{aligned} \tag{1.10}$$

- Let I_1, I_2, ... denote distinct strings of $\{i_t\}_{t=0}^{t=l-1}$ or $\{i_t\}_{t=0}^{t=l}$ satisfying (1.10). For each string I_j, a stabilizing set in (k_i, k_d) space with $k_p = k_p^*$ is given by the intersection of the linear inequalities

$$i_t \cdot \nu_{even}(-\omega_t^2, k_i, k_d) > 0 \tag{1.11}$$

  $\forall t \in \{1, \ldots, l-1\}$ if $n+m$ is odd, or $\forall t \in \{1, \ldots, l\}$ if $n+m$ is even, where each $i_t \in \{-1, +1\}$.

- For each string I_j, the intersection generates either an empty set or a convex polygon $S_j(k_p^*)$. The stabilizing set for a fixed k_p^* is the union of these convex polygons

$$S(k_p^*) = \bigcup_j S_j(k_p^*). \tag{1.12}$$

- The complete stabilizing set in (k_p, k_i, k_d) space can be found by sweeping k_p over the real axis and repeating all of the above calculations. The range of sweeping can be restricted to those values of k_p such that the number of roots $l-1$ can satisfy the signature requirement in the most favorable case:

$$l - 1 \geq \begin{cases} \dfrac{n-m-1+2z^+}{2}, & \text{if } n+m \text{ odd}, \\ \dfrac{n-m-2+2z^+}{2}, & \text{if } n+m \text{ even}. \end{cases} \tag{1.13}$$

Thus, k_p needs to be swept over those ranges where (1.9) is satisfied with $l-1$ given by (1.13).

1.2 Signature Method for Discrete Time Systems

The signature method converts the computation of the stabilizing set into a signature assignment problem for a related rational function, which is computationally more tractable.

Consider a polynomial $\delta(z)$ with real coefficients. Let $\phi_\delta(\theta)$ denote the phase of $\delta(z)$ at $z = e^{j\theta}$. If $\delta(z)$ has i_δ roots in the interior of the unit circle centered at the origin of the complex plane, then the net change in phase $\phi_\delta(\theta)$ as θ runs from 0 to 2π is:

$$\Delta_{\theta=0}^{2\pi}\phi_\delta(\theta) = 2\pi i_\delta.$$

We call i_δ the *Schur signature* of $\delta(z)$. If i_δ is equal to the degree of $\delta(z)$, then we say $\delta(z)$ is *Schur stable*.

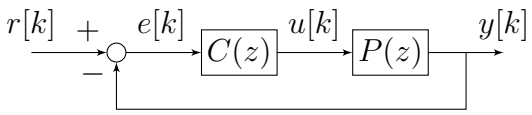

Figure 1.2: Unity feedback control loop in the discrete time domain.

Consider the unity feedback control loop with the controller $C(z)$ and plant $P(z)$ in Fig. 1.2, where

$$P(z) = \frac{N(z)}{D(z)}, \tag{1.14}$$

$$C(z) = \frac{K_2 z^2 + K_1 z + K_0}{z(z-1)}, \tag{1.15}$$

and $D(z)$, $N(z)$ are real-coefficient polynomials in z and $C(z)$ is the transfer function of the PID controller. We assume that $P(1) \neq 0$ since the closed loop cannot be stabilized otherwise. The

characteristic polynomial $\delta(z)$ of the closed loop system is

$$\delta(z) = z(z-1)D(z) + (K_2 z^2 + K_1 z + K_0)N(z). \tag{1.16}$$

Define $\mathcal{S}$ to be the set of all stabilizing PID controllers:

$$\mathcal{S} := \{(K_0, K_1, K_2)\text{: } \delta(z) \text{ is Schur stable}\}. \tag{1.17}$$

We call $\mathcal{S}$ the stabilizing set.

If $Q_1(z)$ and $Q_2(z)$ have i_1, i_2 roots in the interior of the unit circle, respectively, then the Schur signature of $Q(z) := Q_1(z)/Q_2(z)$ is $i_1 - i_2$ since

$$\Delta_{\theta=0}^{\pi} \phi_Q(\theta) = \Delta_{u=-1}^{1} \phi_Q(u) = \pi(i_1 - i_2).$$

The procedure to find the set $\mathcal{S}$ using this signature concept is summarized in the following.

- Consider the controller $C(z)$ of the form in (1.15) for the plant $P(z)$ in (1.14). Multiplying the characteristic polynomial $\delta(z)$ in (1.16) by $z^{-1}N(z^{-1})$, we have the rational function

$$\begin{aligned} Q(z) &:= z^{-1}\delta(z)N(z^{-1}) \\ &= (z-1)D(z)N(z^{-1}) \\ &\quad + (K_2 z + K_1 + K_0 z^{-1})N(z)N(z^{-1}). \end{aligned} \tag{1.18}$$

- Let n, m denote the degrees of $D(z)$, $N(z)$, respectively and m^0 denote the number of roots of $N(z)$ inside the unit circle. The closed loop system is stable ($\delta(z)$ is Schur stable) if and only if the Schur signature of $Q(z)$ is $n - m^0 + 1$.

- To determine the unit circle image of $Q(z)$, let:

$$e^{j\theta} := -u + jv,$$

$$e^{-j\theta} := -u - jv.$$

Using the representations in (3.8), (3.9) we define the following polynomials in $u \in (-1, 1)$:

$$\begin{aligned}
P_1(u) &:= R_D(u)R_N(u) + (1-u^2)T_D(u)T_N(u),\\
P_2(u) &:= R_N(u)T_D(u) - T_N(u)R_D(u),\\
P_3(u) &:= R_N^2(u) + (1-u^2)T_N^2(u).
\end{aligned}$$

- Introducing a new parameter K_3 and two polynomials $R(u, K_1, K_2, K_3)$ and $T(u, K_3)$ in the following:

$$\begin{aligned}
K_3 &:= K_2 - K_0,\\
T(u, K_3) &:= P_1(u) - (u+1)P_2(u) + K_3P_3(u),\\
R(u, K_1, K_2, K_3) &:= -(u+1)P_1(u) - (1-u^2)P_2(u)\\
&\qquad - \{(2K_2 - K_3)u - K_1\}P_3(u),
\end{aligned}$$

  we obtain the unit circle image of $Q(z)$:

$$Q(e^{j\theta}) = R(u, K_1, K_2, K_3) + jvT(u, K_3).$$

  Note that only K_3 appears in $T(u, K_3)$.

- Fix $K_3 = K_3^*$. Let $u_1, \cdots, u_k$ denote the real distinct zeros of $T(u, K_3^*)$ of odd multiplicities for $u \in (-1, 1)$:

$$-1 < u_1 < u_2 < \cdots < u_k < 1.$$

  Denote $u_0 := -1$ and $u_{k+1} := 1$.

- Write

$$\tau := \text{sgn}[T(-1^+, K_3^*)].$$

- Determine the strings of integers $i_0, \ldots, i_{k+1}$ from $\{-1, +1\}$ such that

$$\begin{aligned} & n - m^0 + 1 \\ & = \frac{1}{2}\tau \left(i_0 + 2\sum_{t=1}^{k}(-1)^t i_t + (-1)^{k+1} i_{k+1} \right). \end{aligned} \tag{1.19}$$

- Let I_1, I_2, ... denote distinct strings of $\{i_t\}_{t=0}^{t=k+1}$ satisfying (1.19). For each string I_j, a stabilizing set in (K_1, K_2) space with $K_3 = K_3^*$ is given by the intersection of the linear inequalities

$$i_t \cdot R(u_t, K_1, K_2, K_3^*) > 0, \ \forall\, t \in \{0, \ldots, k+1\}$$

- For each string I_j, the intersection generates either an empty set or a convex polygon $\mathcal{S}_j(K_3^*)$. The stabilizing set for a fixed K_3^* is the union of these convex polygons

$$\mathcal{S}(K_3^*) = \bigcup_j \mathcal{S}_j(K_3^*).$$

- The complete stabilizing set in (K_1, K_2, K_3) space can be found by sweeping K_3 over the real axis and repeating the above calculations. The range of sweeping can be restricted to those values of K_3 such that there is enough number of roots k of $T(u, K_3)$ satisfying (1.19).

- The complete stabilizing set in (K_0, K_1, K_2) space can be found by using the mapping:

$$\begin{bmatrix} K_0 \\ K_1 \\ K_2 \end{bmatrix} = \begin{bmatrix} 0 & 1 & -1 \\ 1 & 0 & 0 \\ 0 & 1 & 0 \end{bmatrix} \begin{bmatrix} K_1 \\ K_2 \\ K_3 \end{bmatrix}.$$

1.3 Notes and References

The stabilizing set was first introduced in [1]. Silva treated the stabilizing set for time-delay plants in [2]. Bhattacharyya, Datta and Keel developed new results on PID in [3].

2. H_∞ OPTIMAL SYNTHESIS FOR CONTINUOUS TIME PLANTS *

2.1 Introduction

The Nyquist stability criterion entails the frequency response of the open loop transfer function to stay away from the critical point $-1 + j0$ in the complex plane. The stability margins such as gain and phase margins are a measure of 'robustness' of a given system as they represent how far the frequency response is away from the critical point at the crossover frequencies. An H_∞ norm specification on the error transfer function measures the closest distance to the critical point from all frequencies. In this chapter, we consider the H_∞ norm on the error transfer function as a design criterion. The complete stabilizing set $\mathcal{S}$ of PI and PID controllers is computed in [3]. Having the set $\mathcal{S}$ in hand, we find the subset $\mathcal{S}_\gamma$ of PI and PID controllers satisfying the H_∞ norm less than γ.

In the next section, we develop a useful relationship between H_∞ norm specification on the error transfer function and guaranteed gain and phase margins. Following this we present our constructive calculation of $\mathcal{S}_\gamma$ for PI or PID controller sets satisfying the given H_∞ norm specification.

2.2 H_∞ Optimal Control and Stability Margins

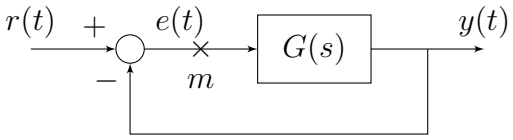

Figure 2.1: Unity feedback loop.

Consider the unity feedback system in Fig. 2.1 with the error transfer function

$$\frac{e(s)}{r(s)} = \frac{1}{1 + G(s)}. \tag{2.1}$$

*Sections 2.2, 2.3, 2.4 and 2.5 © 2018 IFAC. Reproduced with permission from the original publication "PID controller design with an H_∞ criterion", IFAC-PapersOnline, Volume 51, Issue 4, 2018, Pages 400-405. https://doi.org/10.1016/j.ifacol.2018.06.127

Suppose that $G(s)$ includes a controller designed to make the H_∞ norm of (2.1) less than γ, a prescribed real positive number. Then

$$\frac{1}{|1+G(j\omega)|} < \gamma, \qquad \text{for all } \omega \geq 0 \tag{2.2}$$

and (2.2) is equivalent to

$$|1+G(j\omega)| > \frac{1}{\gamma}, \qquad \text{for all } \omega \in [0,\infty). \tag{2.3}$$

We will now establish that (2.3) implies guaranteed gain and phase margins at the loop breaking point 'm' in Fig. 2.1.

Remark 2.1. Let γ^* denote the infimum value of γ satisfying (2.3). When $G(s)$ is strictly proper, $\gamma^* \geq 1$. When $G(s)$ is proper, $\gamma^* > 1/|1+G(j\infty)|$.

Case 1: $\gamma > 1$

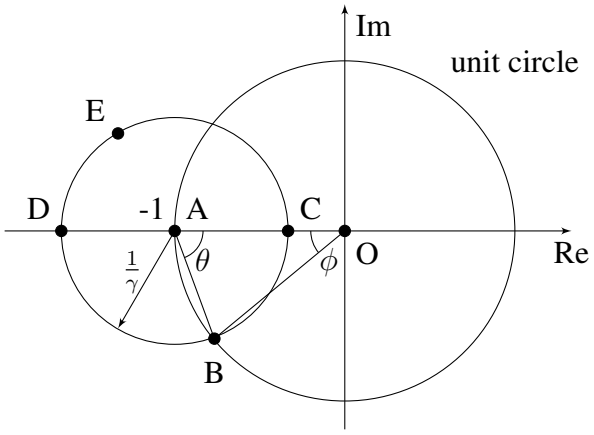

Figure 2.2: $\gamma > 1$. © 2018 IFAC

The condition (2.3) implies that the Nyquist plot $G(j\omega)$ stays out of the circle CEDB centered at $-1+j0$ and of radius $1/\gamma$. In Fig. 2.2, we have the limiting case in which $G(j\omega)$ passes through

B, the phase margin is ϕ and

$$G(j\omega) = \overrightarrow{\text{OB}} \tag{2.4}$$

$$-1 + j0 = \overrightarrow{\text{OA}} \tag{2.5}$$

$$1 + G(j\omega) = \overrightarrow{\text{AB}}. \tag{2.6}$$

Since $\overrightarrow{\text{OA}} + \overrightarrow{\text{AB}} = \overrightarrow{\text{OB}}$, we have

$$-1 + j0 + \frac{1}{\gamma} e^{-j\theta} = -1e^{j\phi}. \tag{2.7}$$

Also

$$2\theta + \phi = \pi \tag{2.8}$$

from the triangle $\overrightarrow{\text{OAB}}$.

From (2.7) and (2.8),

$$-1 + \frac{1}{\gamma} \sin\left(\frac{\phi}{2}\right) = -\cos\phi \tag{2.9}$$

$$\sin\phi = \frac{1}{\gamma} \cos\left(\frac{\phi}{2}\right). \tag{2.10}$$

From (2.10),

$$\phi = 2\sin^{-1}\left(\frac{1}{2\gamma}\right) \tag{2.11}$$

which is the guaranteed minimum phase margin for the H_∞ controller with norm less than γ.

The guaranteed gain margin is the interval:

$$\left[\frac{1}{\text{OD}}, \frac{1}{\text{OC}}\right] = \left[\frac{\gamma}{\gamma+1}, \frac{\gamma}{\gamma-1}\right]. \tag{2.12}$$

Case 2: $\gamma = 1$

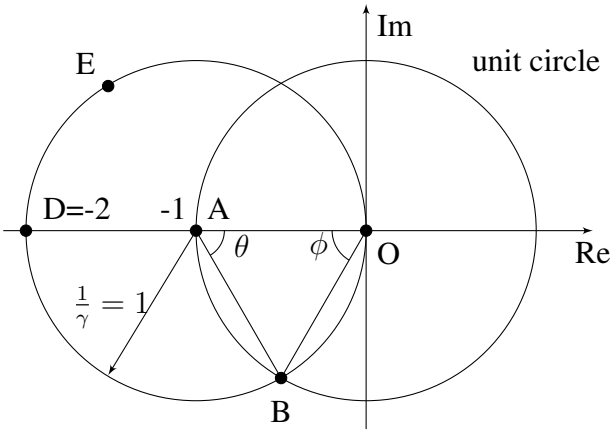

Figure 2.3: $\gamma = 1$. © 2018 IFAC

In this case, Fig. 2.2 is replaced by Fig. 2.3. It is easy to see that the guaranteed phase margin is $\phi = \pi/3$ and the guaranteed gain margin is $\left[\frac{1}{2}, \infty\right]$. These also follow from formulas (2.11) and (2.12) evaluated at $\gamma = 1$.

Case 3: $\gamma < 1$

The geometry corresponding to this case is shown in Fig. 2.4 below.

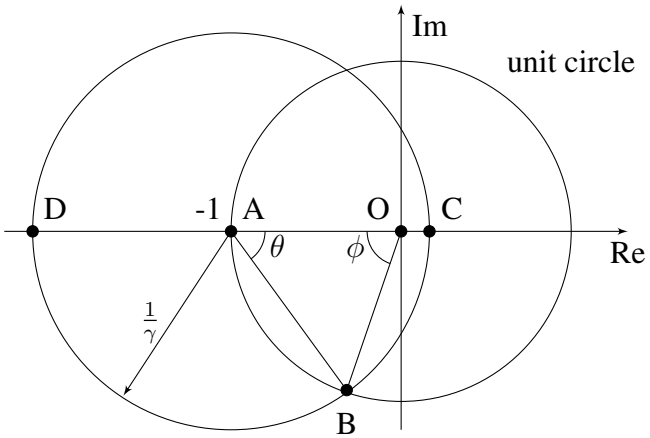

Figure 2.4: $\gamma < 1$. © 2018 IFAC

In this case, it also follows that the guaranteed phase margin is

$$\phi = 2\sin^{-1}\left(\frac{1}{2\gamma}\right) \tag{2.13}$$

and the guaranteed gain margin is

$$\left[\frac{1}{\text{OD}}, \infty\right] = \left[\frac{\gamma}{1+\gamma}, \infty\right]. \tag{2.14}$$

Combining the above cases, we have the following result.

Theorem 2.2. *Consider the unity feedback system in Fig. 2.1. If the H_∞ norm of the error transfer function is less than γ:*

$$\left\| \frac{1}{1+G(s)} \right\|_\infty < \gamma, \tag{2.15}$$

then the guaranteed phase margin at the loop breaking point 'm' is:

$$\phi = 2\sin^{-1}\left(\frac{1}{2\gamma}\right). \tag{2.16}$$

The guaranteed gain margin is:

$$g_m = \begin{cases} \left[\dfrac{\gamma}{\gamma+1}, \dfrac{\gamma}{\gamma-1}\right], & \textit{for} \quad \gamma > 0 \\ \\ \left[\dfrac{\gamma}{\gamma+1}, \infty\right], & \textit{for} \quad \gamma \leq 0 \end{cases} \tag{2.17}$$

Now consider the control system in Fig. 2.5 where $r(t)$ is the reference signal, $e(t)$ the error signal, $u(t)$ the input signal (to the plant), $y(t)$ the output signal, $P(s)$ is the plant transfer function and $C(s)$ is the controller transfer function which we will consider to be either PI or PID.

The problem to be solved in this chapter is: Find the set $\mathcal{S}_\gamma$ of all stabilizing PI or PID con-

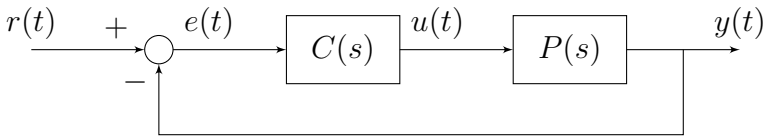

Figure 2.5: Unity feedback control loop.

trollers satisfying

$$\left\| \frac{1}{1 + P(s)C(s)} \right\|_\infty < \gamma. \tag{2.18}$$

In the following two sections we develop the computation of $\mathcal{S}_\gamma$ for PI and PID controllers. Note that (2.18) is equivalent to

$$|1 + P(j\omega)C(j\omega)| > \frac{1}{\gamma}, \quad \forall\, \omega \in [0, \infty). \tag{2.19}$$

2.3 Computation of $\mathcal{S}_\gamma$ for PI Controllers

PI controllers have the form:

$$C(s) = k_p + \frac{k_i}{s}. \tag{2.20}$$

Write

$$P(j\omega) = P_r(\omega) + j\omega P_i(\omega), \tag{2.21}$$

$$C(j\omega) = k_p - j\frac{k_i}{\omega}. \tag{2.22}$$

Substituting (2.21) and (2.22) in (2.19) we get

$$|1 + \underbrace{k_p P_r(\omega) + k_i P_i(\omega)}_{L_0(\omega)} + j(\underbrace{\omega k_p P_i(\omega) - \frac{k_i}{\omega} P_r(\omega)}_{L_1(\omega)})| > \frac{1}{\gamma} \tag{2.23}$$

which can be rewritten as

$$(1 + L_0(\omega))^2 + L_1^2(\omega) > \frac{1}{\gamma^2} \tag{2.24}$$

$$\begin{bmatrix} P_r(\omega) & P_i(\omega) \\ \omega P_i(\omega) & -\frac{P_r(\omega)}{\omega} \end{bmatrix} \begin{bmatrix} k_p \\ k_i \end{bmatrix} = \begin{bmatrix} L_0(\omega) \\ L_1(\omega) \end{bmatrix}. \tag{2.25}$$

(2.25) has a unique solution if

$$|P(j\omega)| \neq 0, \tag{2.26}$$

that is the plant has no $j\omega$ axis zeros.

Assuming (2.26), (2.25) can be solved:

$$\begin{bmatrix} k_p \\ k_i \end{bmatrix} = \underbrace{\frac{1}{|P(j\omega)|^2} \begin{bmatrix} P_r(\omega) & \omega P_i(\omega) \\ -\omega^2 P_i(\omega) & -\omega P_r(\omega) \end{bmatrix}}_{T(\omega)} \begin{bmatrix} L_0(\omega) \\ L_1(\omega) \end{bmatrix} \tag{2.27}$$

(2.24) represents the outside of a circle C_γ of radius $\frac{1}{\gamma}$ in the (L_0, L_1) plane centered at $(-1, 0)$:

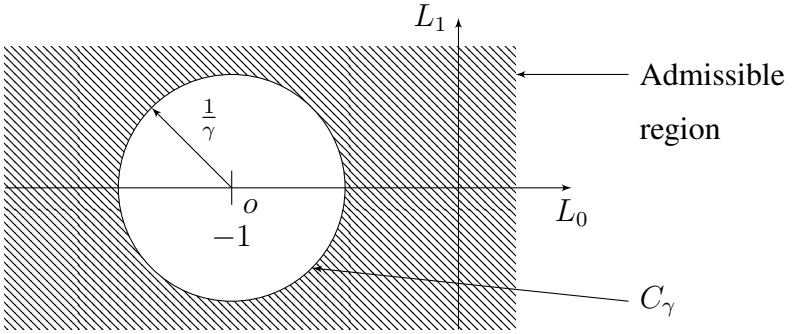

Figure 2.6: The C_γ circle. © 2018 IFAC

Lemma 2.3. *Condition* (2.19) *at a fixed* ω *is equivalent to* k_p, k_i *lying in the exterior of the axis*

parallel ellipse $E_\gamma(\omega)$ *with center* o' *at* $(\frac{-\omega^2 P_i(\omega)}{|P(j\omega)|^2}, \frac{-P_r(\omega)}{|P(j\omega)|^2})$*, and major and minor axes of lengths* $\frac{2}{\gamma|P(j\omega)|}, \frac{2\omega}{\gamma|P(j\omega)|}$.

Proof. For each $\omega \geq 0$, (2.23) is

$$\begin{aligned}
&\left|1 + (P_r(j\omega) + j\omega P_i(j\omega))(k_p - j\frac{k_i}{\omega})\right| > \frac{1}{\gamma} \\
\Leftrightarrow &(1 + P_r(j\omega)k_p + P_i(j\omega)k_i)^2 + \left(\omega P_i(j\omega)k_p - P_r(j\omega)\frac{k_i}{\omega}\right)^2 > \frac{1}{\gamma^2} \\
\Leftrightarrow &\frac{(k_i - c_1)^2}{a^2} + \frac{(k_p - c_2)^2}{b^2} > 1
\end{aligned} \tag{2.28}$$

where

$$c_1 = \frac{-\omega^2 P_i(\omega)}{|P(j\omega)|^2},\ c_2 = \frac{-P_r(\omega)}{|P(j\omega)|^2},\ a = \frac{\omega/\gamma}{|P(j\omega)|},\ b = \frac{1/\gamma}{|P(j\omega)|}. \tag{2.29}$$

□

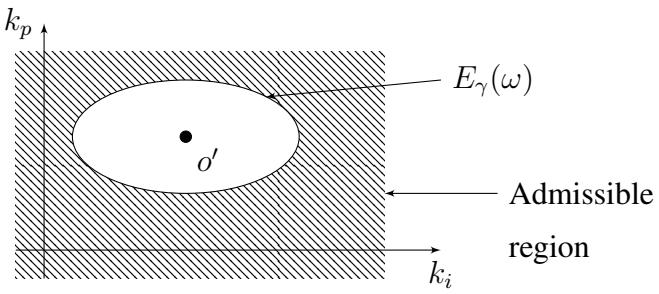

Figure 2.7: The $E_\gamma(\omega)$ ellipse. © 2018 IFAC

For a fixed ω, let $\mathcal{S}_\gamma(\omega)$ denote the intersection of the stabilizing set S with the exterior of the ellipse $E_\gamma(\omega)$ as shown in Fig. 2.8. In other words,

$$\mathcal{S}_\gamma(\omega) = \mathcal{S} \setminus E_\gamma(\omega)\ \ \forall\, \omega \in [0, \infty). \tag{2.30}$$

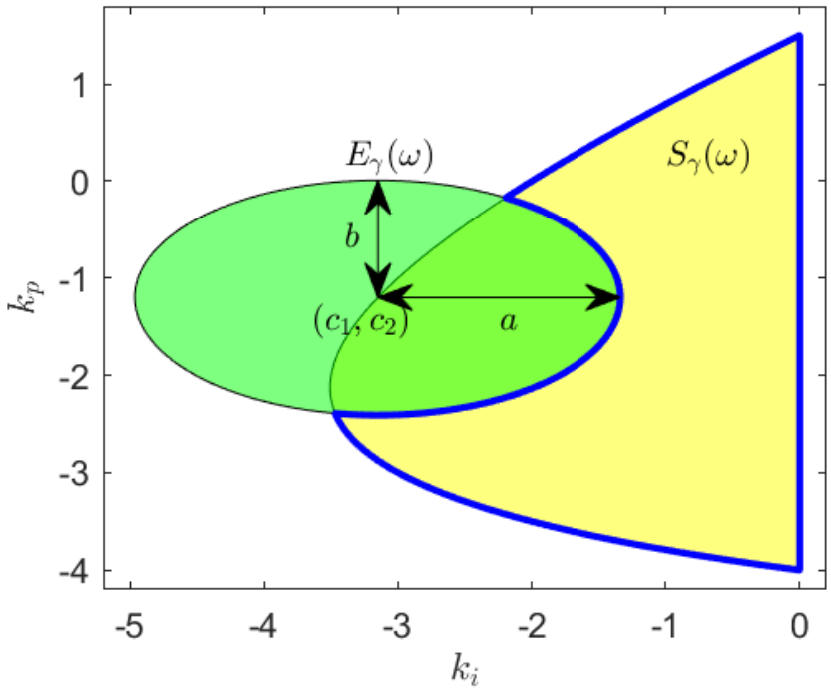

Figure 2.8: $E_\gamma(\omega)$ and $S_\gamma(\omega)$. © 2018 IFAC

Since (2.19) must hold for all ω,

$$\mathcal{S}_\gamma = \bigcap_{\omega=0}^{\infty} \mathcal{S}_\gamma(\omega) \tag{2.31}$$

as shown in Fig. 2.9.

We state this result in the following theorem.

Theorem 2.4. *In the unity feedback control loop, suppose that the plant $P(s)$ has no $j\omega$ axis zeros. All stabilizing PI controllers $C(s)$ satisfying the H_∞ norm bound of γ on the error transfer function is the set $\mathcal{S}_\gamma$:*

$$\mathcal{S}_\gamma = \bigcap_{\omega=0}^{\infty} \mathcal{S}_\gamma(\omega). \tag{2.32}$$

Proof. $\mathcal{S}_\gamma(\omega)$ is the admissible set for each ω and the controller must satisfy the H_∞ norm for all frequencies. Hence we have the set $\mathcal{S}_\gamma$ by intersecting the admissible sets $\mathcal{S}_\gamma(\omega)$ for all ω. □

Note that $\mathcal{S}$ can be determined using the concept of signature developed in [3]. If $E_\gamma(\omega)$ is

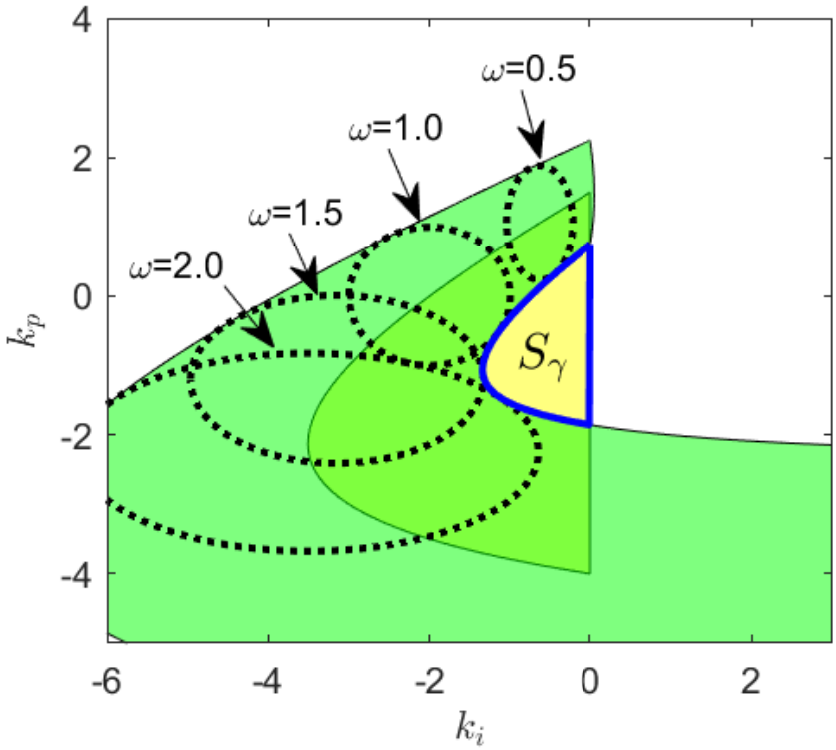

Figure 2.9: $\mathcal{S}_\gamma$. © 2018 IFAC

outside of $\mathcal{S}$ then $\mathcal{S}_\gamma(\omega) = S$. If $\mathcal{S} \subset E_\gamma(\omega)$ then $\mathcal{S}_\gamma$ is empty.

Remark 2.5. We can determine the minimum achievable γ for a given plant under PI or PID control. The minimum γ denoted γ^*, is the value for which the union of family of ellipses eclipses the stabilizing set $\mathcal{S}$.

Remark 2.6. The computation of $\mathcal{S}_\gamma$ would not be possible without knowing the stabilizing set $\mathcal{S}$.

2.4 Computation of $\mathcal{S}_\gamma$ for PID Controllers

PID controllers are of form:

$$C(s) = k_p + \frac{k_i}{s} + k_d s. \tag{2.33}$$

Substituting $s = j\omega$, we have

$$C(j\omega) = k_p - j\frac{1}{\omega}\left(k_i - \omega^2 k_d\right). \tag{2.34}$$

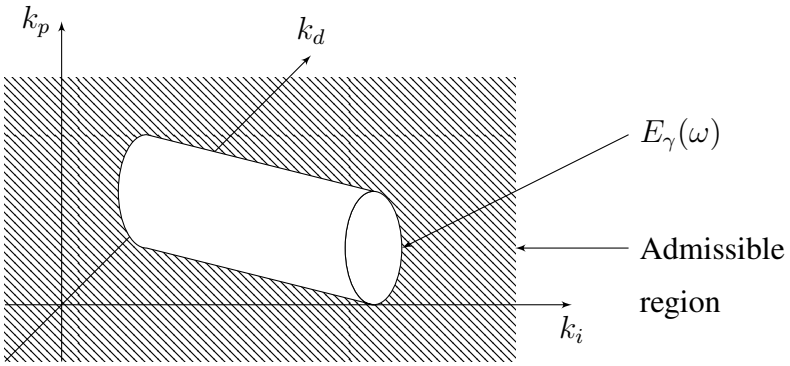

Figure 2.10: The $E_\gamma(\omega)$ elliptic cylinder. © 2018 IFAC

Notice that (2.34) is equal to (2.22) if we replace k_i in (2.22) with $k_i' = k_i - \omega^2 k_d$. By analysis similar to the PI case, it is easy to show that (2.19) implies that the controller parameters k_p, k_i, k_d must lie in the exterior of $E_\gamma(\omega)$ described by:

$$\frac{(k_i - \omega^2 k_d - c_1)^2}{a^2} + \frac{(k_p - c_2)^2}{b^2} > 1 \tag{2.35}$$

where $E_\gamma(\omega)$ is an elliptic cylinder with the center lying on the line

$$\begin{cases} k_i - \omega^2 k_d = \dfrac{-\omega^2 P_i(\omega)}{|P(j\omega)|^2}, \\ k_p = \dfrac{-P_\gamma(\omega)}{|P(j\omega)|^2}, \end{cases} \tag{2.36}$$

and major and minor axes $\dfrac{2}{\gamma|P(j\omega)|}$ and $\dfrac{2\omega}{\gamma\sqrt{\omega^4+1}|P(j\omega)|}$.

As before,

$$\mathcal{S}_\gamma(\omega) = \mathcal{S} \setminus E_\gamma(\omega) \;\; \forall\, \omega \in [0, \infty) \tag{2.37}$$

and

$$\mathcal{S}_\gamma = \bigcap_{\omega=0}^{\infty} \mathcal{S}_\gamma(\omega). \tag{2.38}$$

Remark 2.7. We can also consider the H_∞ norm with a weighting function $W(s)$ multiplied by the error transfer function in (2.18). In this case, we may replace γ by γ' where $\gamma' = \dfrac{\gamma}{|W(j\omega)|}$. Then, the major and minor axes of the axis parallel ellipse $E_\gamma(\omega)$ are subject to change with ω in accordance to the frequency response of the weighting function. However, the rest of the derivation of the equations in this section remains the same.

Remark 2.8. If $C(s)$ is replaced by

$$C_\tau(s) = \frac{k_p s + k_i + k_d s^2}{s(\tau s + 1)}, \tag{2.39}$$

then

$$C_\tau(s)P(s) = C(s)\frac{1}{\tau s + 1}P(s). \tag{2.40}$$

Since τ can be fixed a priori, replace $P_r(j\omega)$ and $P_i(j\omega)$ by

$$P_r'(j\omega) = \frac{P_r(j\omega) + \tau\omega^2 P_i(j\omega)}{1 + \tau^2\omega^2}$$
$$P_i'(j\omega) = \frac{P_i(j\omega) - \tau P_r(j\omega)}{1 + \tau^2\omega^2}.$$

Then, the controller design can be carried out as before.

2.5 Examples

We present two examples to illustrate the steps to find the set S_γ.

Example 2.9. Consider the second order plant and the PI controller:

$$P(s) = \frac{s-2}{s^2 + 4s + 3}, \;\; C(s) = k_p + \frac{k_i}{s}. \tag{2.41}$$

The stabilizing set was first computed for the plant and the PI controller given in (2.41). The family of ellipses $E_\gamma(\omega)$ were drawn by sweeping over ω and $\mathcal{S}_\gamma$ was found accordingly for $\gamma =$ 1.6, 2.0, 4.0 and 8.0. In Fig. 2.11 we observed that $\mathcal{S}_\gamma$ were contained in the stabilizing set $\mathcal{S}$ and

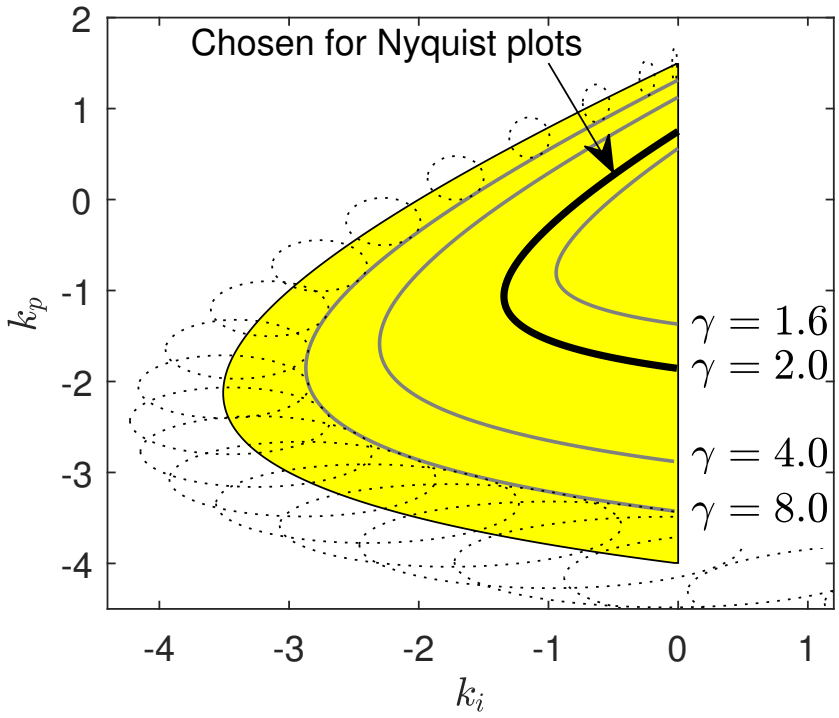

Figure 2.11: $\mathcal{S}_\gamma$ for $\gamma = 1.6, 2.0, 4.0, 8.0$ with the stabilizing set. © 2018 IFAC

$\mathcal{S}_{\gamma_1} \subset \mathcal{S}_{\gamma_2}$ if $\gamma_1 < \gamma_2$. So, $\mathcal{S}_\gamma$ for $\gamma \in [1,\ \infty)$ is the telescoping series of sets shown. If k_p, k_i were chosen from sets $\mathcal{S}_\gamma$, the Nyquist plot must stay outside of a circle centered at the critical point $-1 + j0$ with radius of $1/\gamma$. We chose some boundary points in $\mathcal{S}_\gamma$ that were inside the stabilizing set $\mathcal{S}$ where $\gamma = 2$ and drew the Nyquist plots in Fig. 2.12. Each Nyquist plot was at least 0.5 away from the critical point.

Following Theorem 2.2, the guaranteed gain margin was

$$\left[\frac{\gamma}{\gamma+1},\ \ \frac{\gamma}{\gamma-1}\right] = \left[\frac{2}{3},\ \ 2\right], \tag{2.42}$$

and the guaranteed phase margin ϕ was

$$\phi = 2\sin^{-1}\left(\frac{1}{2\gamma}\right) = 28.955^o \tag{2.43}$$

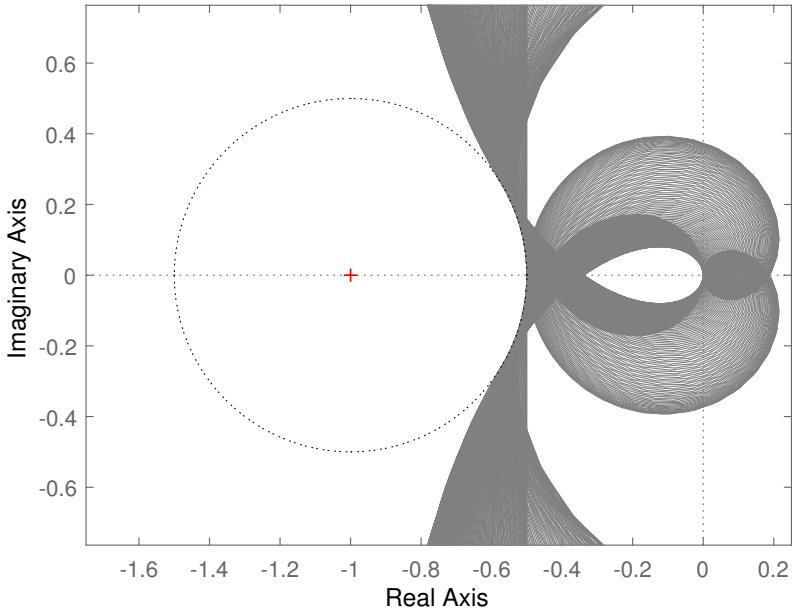

Figure 2.12: Nyquist plots with k_p, k_i along the curve of $\gamma = 2$. © 2018 IFAC

for $\gamma = 2$. Fig. 2.13 shows the guaranteed gain and phase margins when we choose k_p and k_i from S_γ for $\gamma = 2$. For all controllers achieving the same H_∞ norm at the boundary of S_γ, there is a trade off between gain and phase margins. When higher gain margin is desired, one should sacrifice some phase margin and vice versa. Nevertheless with the H_∞ norm we get the guaranteed gain and phase margins calculated in Eqs. (2.42) and (2.43).

Example 2.10. Consider a rational plant transfer function and the PID controller:

$$P(s) = \frac{10s^3 + 9s^2 + 362.4s + 36.16}{2s^5 + 2.7255s^4 + 138.4292s^3 + 156.471s^2 + 637.6472s + 360.1779} \tag{2.44}$$

$$C(s) = k_p + \frac{k_i}{s} + k_d s. \tag{2.45}$$

The stabilizing set was computed using the signature method and is shown in Fig. 2.14. We chose $k_d = 9$ and computed $\mathcal{S}_\gamma$ for $\gamma = 1$ in the k_p, k_i plane. Fig. 2.15 shows S_γ and the family of

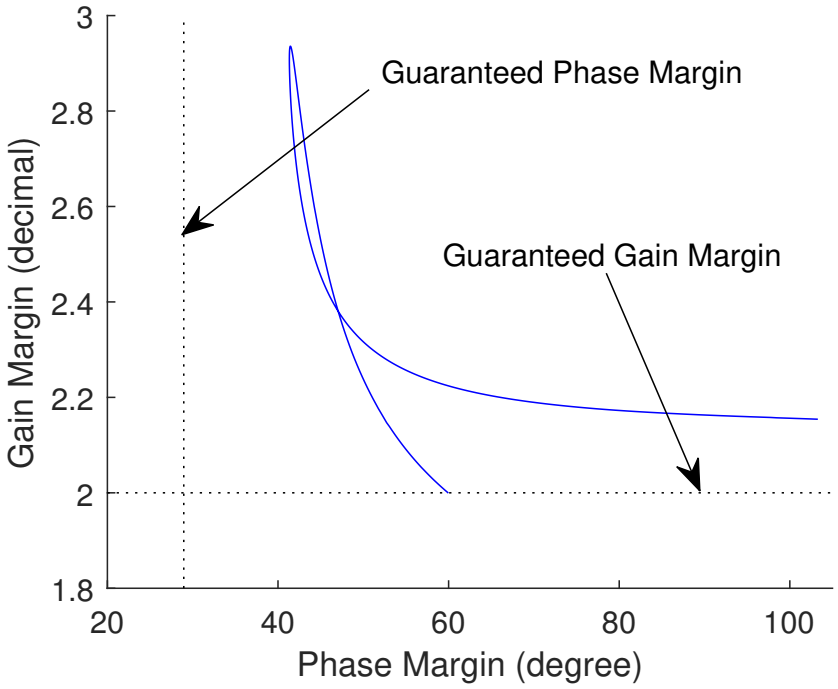

Figure 2.13: Guaranteed gain and phase margin of the boundary points of $\mathcal{S}_\gamma$ for $\gamma = 2$. © 2018 IFAC

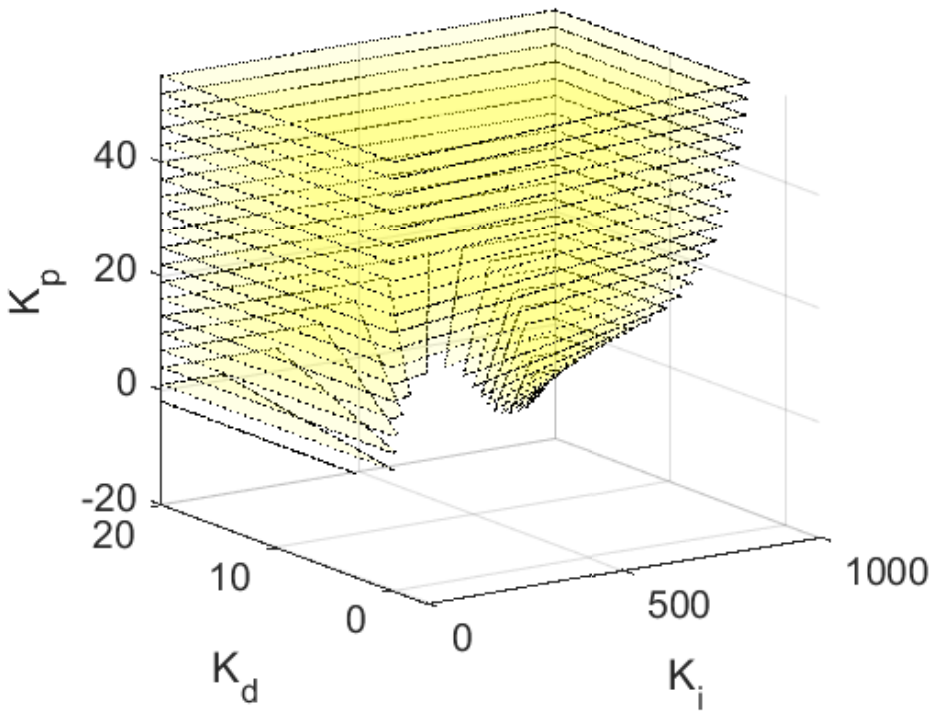

Figure 2.14: The stabilizing set in k_p, k_i, k_d space using the signature method. © 2018 IFAC

ellipses, $E_\gamma(\omega)$.

We observed that the stabilizing set with $k_d = 9$ was unbounded in the k_p, k_i plane. However, $\mathcal{S}_\gamma$ for $\gamma = 1$ in the same plane was bounded. For high values of ω the major and minor axes of the ellipses grow as the centers c_1 and c_2 in (2.29) go away from the origin. So, we suggest that the family of ellipses be computed for high enough values of ω to get the exact set $\mathcal{S}_\gamma$.

Clearly in this case, $\mathcal{S}_\gamma$ is not empty and the H_∞ norm condition less than $\gamma = 1$ provides very good robustness, namely $[0.5, \infty]$ gain margin and 60^o phase margin. All of the points in $\mathcal{S}_\gamma$ guarantee such good robustness. In fact, since the open loop transfer function $P(s)C(s)$ is strictly proper, the Nyquist plot of $P(j\omega)C(j\omega)$ goes to 0 as $\omega \to \infty$ and so every point in $\mathcal{S}_\gamma$ achieves the same H_∞ norm.

Time response considerations

So far we have discussed stability and robustness. However, the design of a controller should

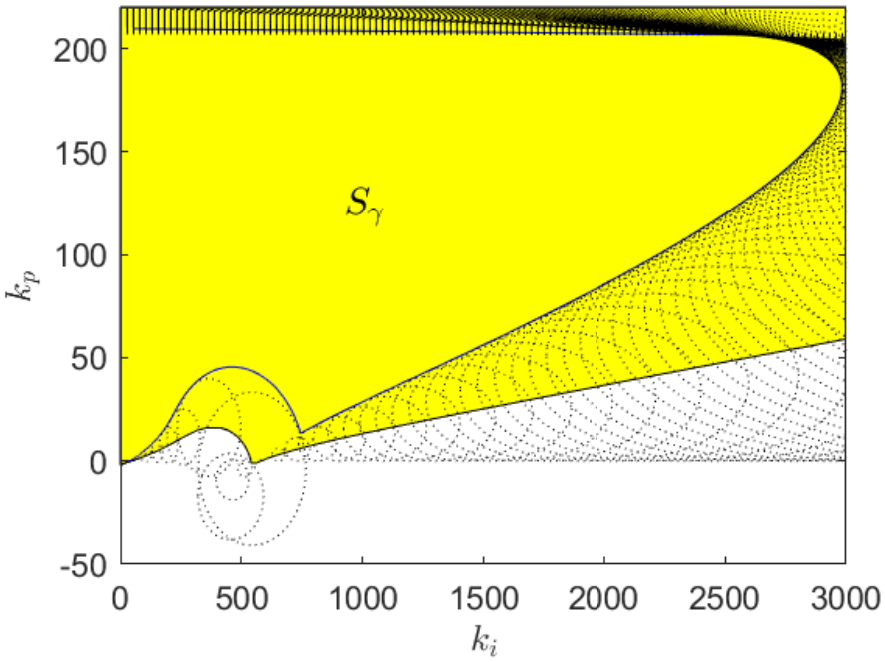

Figure 2.15: S_γ and family of ellipses for $\gamma = 1$ in k_p, k_i plane with $k_d = 9$. © 2018 IFAC

pay attention to the time response. In order to demonstrate this, we chose the following three design points:

$$\begin{cases} C_1(s) = 185 + \dfrac{2986}{s} + 9s, \\ C_2(s) = 20 + \dfrac{800}{s} + 9s, \\ C_3(s) = 19 + \dfrac{200}{s} + 9s. \end{cases} \tag{2.46}$$

The first point has the maximum k_i value in $\mathcal{S}_\gamma$, the second and the third are arbitrary points from the boundary of $\mathcal{S}_\gamma$.

The Nyquist plots in Fig. 2.16 confirms that all three design points satisfy the robustness condition. The step responses in Fig. 2.17 shows that the three controller designs result in different time responses in terms of overshoot and settling time. While $C_1(s)$ and $C_2(s)$ have highest and intermediate integral gains, $C_3(s)$ provides much shorter settling time and lower overshoot than the other two controllers do.

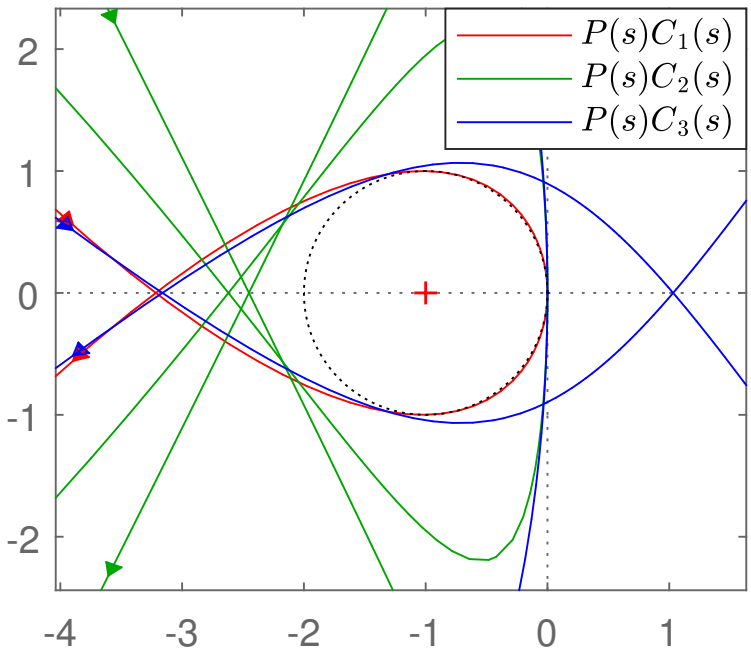

Figure 2.16: Nyquist diagram for $P(s)C_1(s)$ (red), $P(s)C_2(s)$ (green) and $P(s)C_3(s)$ (blue).

The integrator in the controller provided zero steady state error and we found all stabilizing controllers achieving prescribed H_∞ norm of the error transfer function. While the robustness and zero steady state error could be achieved by the proposed method, one should also consider the quality of the transient response when tuning the PID parameters within the set $\mathcal{S}_\gamma$. Thus, PID controller design for better transient response within the same degree of robustness is an important area of research.

2.6 Notes and References

The main results of this chapter are taken from Han, Keel, and Bhattacharyya [4]. In [5], the 2D regions of stabilizing PID controllers achieving the H_∞ norm bound of γ on the sensitivity and complementary sensitivity functions with weightings were found by using Neimark's D-decomposition. The difference is that our approach explicitly uses the *stabilizing set*. A simi-

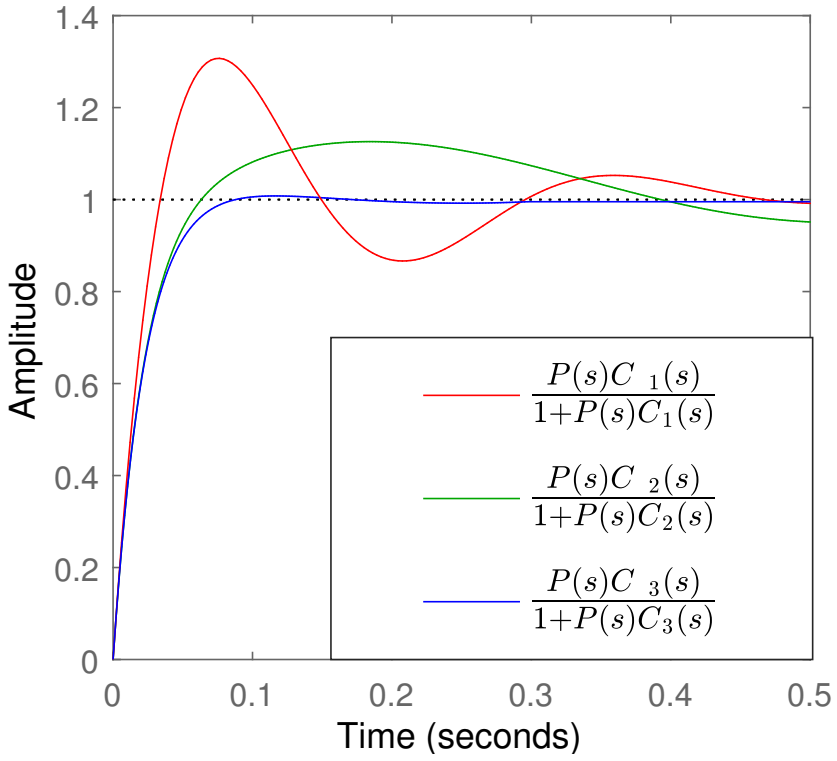

Figure 2.17: Step responses for the closed loop systems of $P(s)C_1(s)$ (red), $P(s)C_2(s)$ (green) and $P(s)C_3(s)$ (blue). © 2018 IFAC

lar approach was adopted in [6] for first order controllers and in this case the stability region was computed a priori. In [7] it was shown that at a fixed frequency (and for a fixed k_d, the derivative gain) the L_2 norm of the error transfer function being equal to γ was represented by an ellipse in (k_p, k_i) space. An H_∞ optimal PID design using a frequency loop-shaping approach was reported in [8, 9].

3. H_∞ OPTIMAL SYNTHESIS FOR DISCRETE TIME PLANTS

In this chapter, we consider the H_∞ optimal synthesis of digital PI and PID controllers. We present the computation of $\mathcal{S}_\gamma$, the set of stabilizing digital PI or PID controllers for a given plant, satisfying an H_∞ norm bound of γ on the error transfer function.

3.1 Introduction

In digital control, dynamic systems are often represented in terms of z-transforms of discrete-time signals and systems. In this chapter we extend the H_∞ norm approach for the design of continuous time systems developed in Chapter 2 to discrete-time systems. The H_∞ norm criterion on the error transfer function is written in terms of the z-transforms of discrete-time signals and systems. We compute the stabilizing set $\mathcal{S}$ of digital PI or PID controllers based on the results in [3]. Having computed the stabilizing set $\mathcal{S}$, we constructively determine the subset $\mathcal{S}_\gamma$ of digital PI or PID controllers for which the error transfer function of the closed loop system has an H_∞ norm less than a prescribed real value $\gamma > 0$.

3.2 Computation of $\mathcal{S}_\gamma$ for Digital PI Controllers

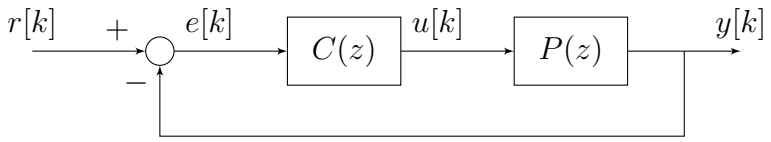

Figure 3.1: Unity feedback control loop in the discrete time domain.

Consider the unity feedback loop with a discrete time controller and plant in Fig. 3.1, where

$$P(z) = \frac{N(z)}{D(z)}, \tag{3.1}$$

$$C(z) = \frac{K_1 z + K_0}{z - 1}, \tag{3.2}$$

and $D(z)$, $N(z)$ are polynomials in z with real coefficients and $C(z)$ is the transfer function of a PI controller. We assume that $P(1) \neq 0$ since the closed loop cannot be stabilized otherwise. The error transfer function is

$$\frac{E(z)}{R(z)} = \frac{1}{1 + P(z)C(z)} \tag{3.3}$$

where $E(z)$ and $R(z)$ are the z-transforms of $e[k]$ and $r[k]$, respectively.

The H_∞ norm criterion on the error transfer function is

$$\left\| \frac{E(z)}{R(z)} \right\|_\infty < \gamma \tag{3.4}$$

for a prescribed $\gamma > 0$. This is equivalent to

$$\sup_\theta \left| \frac{1}{1 + P(e^{j\theta})C(e^{j\theta})} \right| < \gamma, \quad \forall\, \theta \in [0, 2\pi)\,. \tag{3.5}$$

Since $N(z)$ and $D(z)$ have real coefficients, it is sufficient to consider $\theta \in [0, \pi)$. Substituting $z = e^{j\theta}$, we have

$$N(z)\big|_{z=e^{j\theta}} = N(e^{j\theta}) \tag{3.6}$$

$$D(z)\big|_{z=e^{j\theta}} = D(e^{j\theta}). \tag{3.7}$$

Writing $u := -\cos\theta$, we decompose (3.6) and (3.7) into real and imaginary parts:

$$N(e^{j\theta})\big|_{-u=\cos\theta} =: R_N(u) + j\sqrt{1-u^2}T_N(u) \tag{3.8}$$

$$D(e^{j\theta})\big|_{-u=\cos\theta} =: R_D(u) + j\sqrt{1-u^2}T_D(u). \tag{3.9}$$

Denoting $v := \sqrt{1-u^2}$,

$$P(e^{j\theta})\big|_{-u=\cos\theta} := \frac{R_N(u) + jvT_N(u)}{R_D(u) + jvT_D(u)}. \tag{3.10}$$

Define $R_P(u)$ and $T_P(u)$ for $P(e^{j\theta})$ similar to those in (3.8) and (3.9). Then,

$$P(e^{j\theta})\big|_{-u=\cos\theta} = R_P(u) + jvT_P(u) =: P(u) \tag{3.11}$$

where

$$R_P(u) = \frac{R_N(u)R_D(u) + v^2T_N(u)T_D(u)}{R_D(u)R_D(u) + v^2T_D(u)T_D(u)}, \tag{3.12}$$

$$T_P(u) = \frac{T_N(u)R_D(u) - R_N(u)T_D(u)}{R_D(u)R_D(u) + v^2T_D(u)T_D(u)}. \tag{3.13}$$

Now, for $C(z)$, we have

$$C(z)|_{z=e^{j\theta}} = C(e^{j\theta}) = \frac{K_1e^{j\theta} + K_0}{e^{j\theta} - 1}. \tag{3.14}$$

By substituting $u = -\cos\theta$ and denoting $v = \sqrt{1-u^2}$, we have

$$\begin{aligned}
C(e^{j\theta}) =& \frac{K_1e^{j\theta} + K_0}{e^{j\theta} - 1},\\
=& \frac{K_1(-u+jv) + K_0}{(-u+jv) - 1},\\
=& \frac{K_0 - K_1u + jvK_1}{-(u+1) + jv},\\
=& \frac{(K_0 - K_1u + jvK_1)(u+1+jv)}{-\{(u+1)^2 + (1-u^2)\}},\\
=& \frac{(u+1)(K_0 - K_1u) - v^2K_1 + jv(K_1(u+1) + K_0 - K_1u)}{-\{u^2 + 2u + 1 + 1 - u^2\}},\\
=& \frac{-1}{2(u+1)}\left[(u+1)\left\{(K_0 - K_1u) - (1-u)K_1\right\} + jv(K_0 + K_1)\right],\\
=& \frac{-1}{2}(K_0 - K_1) - j\frac{v}{2(1+u)}(K_0 + K_1),\\
=& \underbrace{\frac{1}{2}(K_1 - K_0)}_{=:L_0} - j\frac{v}{u+1}\underbrace{\frac{1}{2}(K_0 + K_1)}_{=:L_1},
\end{aligned}$$

where

$$\begin{aligned} L_0 &= -\frac{1}{2}K_0 + \frac{1}{2}K_1, \\ L_1 &= \frac{1}{2}K_0 + \frac{1}{2}K_1. \end{aligned} \tag{3.15}$$

or

$$\begin{bmatrix} L_0 \\ \\ L_1 \end{bmatrix} = \underbrace{\begin{bmatrix} -\frac{1}{2} & \frac{1}{2} \\ \\ \frac{1}{2} & \frac{1}{2} \end{bmatrix}}_{=:W} \begin{bmatrix} K_0 \\ \\ K_1 \end{bmatrix}. \tag{3.16}$$

Notice that the mapping $W : (K_0, K_1) \to (L_0, L_1)$ is invertible and

$$W^{-1} = \begin{bmatrix} -1 & 1 \\ \\ 1 & 1 \end{bmatrix}. \tag{3.17}$$

Thus, we can represent $C(z)|_{z=e^{j\theta}}$ as a function of u, L_0, and L_1:

$$C(u, L_0, L_1) = L_0 - j\frac{v}{u+1}L_1, \tag{3.18}$$

and we simply denote

$$\begin{aligned} C(u) &:= C(u, L_0, L_1) \\ P(u) &:= R_P(u) + j\, v\, T_P(u). \end{aligned}$$

Condition (3.5) is then equivalent to

$$\max_{-1 \le u < 1} \left| \frac{1}{1 + P(u)C(u)} \right| < \gamma. \tag{3.19}$$

For a fixed $u \in [-1, 1)$,

$$\begin{aligned}
&\left|\frac{1}{1+P(u)C(u)}\right| < \gamma, \\
\Leftrightarrow &\left|1+(R_P(u)+jvT_P(u))(L_0 - j\frac{v}{u+1}L_1)\right| > \frac{1}{\gamma}, \\
\Leftrightarrow &\left(1+R_P(u)L_0+\frac{v^2}{u+1}T_P(u)L_1\right)^2 \\
&+v^2\left(T_P(u)L_0-\frac{1}{u+1}R_P(u)L_1\right)^2 > \frac{1}{\gamma^2}. \qquad (3.20)
\end{aligned}$$

Since $|P(u)|^2 = R_P^2(u) + v^2T_P^2(u)$, it is easy to show that (3.20) is equivalent to

$$\frac{\left(L_0+\frac{R_P(u)}{|P(u)|^2}\right)^2}{\frac{1}{\gamma^2|P(u)|^2}} + \frac{\left(L_1+\frac{(u+1)T_P(u)}{|P(u)|^2}\right)^2}{\frac{(u+1)^2}{\gamma^2v^2|P(u)|^2}} > 1. \qquad (3.21)$$

Thus, condition (3.21) is equivalent to L_0, L_1 lying in the complement of the interior of the axis parallel ellipse $F_\gamma(u)$ with center o at $\left(\frac{-R_P(u)}{|P(u)|^2}, \frac{-(u+1)T_P(u)}{|P(u)|^2}\right)$, principal axes $\frac{2}{\gamma|P(u)|}$, $\frac{2|u+1|}{\gamma\, v\, |P(u)|}$ in (L_0, L_1) space. This is illustrated in Fig. 3.2.

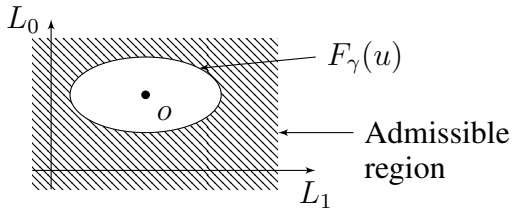

Figure 3.2: The $F_\gamma(u)$ ellipse.

We can use W^{-1} in (3.17) to map $F_\gamma(u)$ back to (K_0, K_1) space. Denoting by $E_\gamma^o(u)$ the interior of the ellipse in (K_0, K_1) space, we define $S_\gamma(u)$, a subset of the stabilizing set $\mathcal{S}$ for a

fixed $u \in (-1, 1)$ as follows:

$$\mathcal{S}_\gamma(u) := \mathcal{S} \setminus \left(E^o_\gamma(u) \cap \mathcal{S}\right), \ \forall\, u \ \in \ (-1, 1). \tag{3.22}$$

We state the main result in the following theorem.

Theorem 3.1. *In the unity feedback control loop with the controller $C(z)$ and plant $P(z)$, suppose that $P(1) \neq 0$. All stabilizing PI controllers $C(z)$ satisfying the H_∞ norm bound of γ on the error transfer function is the set S_γ:*

$$\mathcal{S}_\gamma = \bigcap_{u \in (-1,1)} \mathcal{S}_\gamma(u). \tag{3.23}$$

Proof. $\mathcal{S}_\gamma(u)$ is the admissible set for each u and (3.19) must be satisfied for all $u \in (-1, 1)$. Hence the set $\mathcal{S}_\gamma$ is obtained by intersecting the admissible sets $\mathcal{S}_\gamma(u)$ for all $u \in (-1, 1)$. □

Fact 3.2. If $0 < \gamma_1 \leq \gamma_2$, then $\mathcal{S}_{\gamma_1} \subseteq \mathcal{S}_{\gamma_2}$.

Remark 3.3. By Fact 3.2, the minimum achievable γ denoted by γ^* can be constructively determined for a given plant.

3.3 Computation of $\mathcal{S}_\gamma$ for Digital PID Controllers

Consider a unity feedback control loop with a plant and a controller in Fig. 1.2, where

$$P(z) = \frac{N(z)}{D(z)}, \tag{3.24}$$

$$C(z) = \frac{K_2 z^2 + K_1 z + K_0}{z(z-1)}, \tag{3.25}$$

$D(z)$, $N(z)$ are polynomials in z with real coefficients and $C(z)$ is the same transfer function representation for a PID controller. Again, it is assumed that $P(1) \neq 0$, since stabilization is impossible otherwise.

Now, for $C(z)$, we have

$$C(z)\big|_{z=e^{j\theta}} = C(e^{j\theta}) = \frac{K_2 e^{2j\theta} + K_1 e^{j\theta} + K_0}{e^{j\theta}(e^{j\theta} - 1)} = \frac{K_2 e^{j\theta} + K_1 + K_0 e^{-j\theta}}{e^{j\theta} - 1}. \tag{3.26}$$

By substituting $u = -\cos\theta$ and $v = \sqrt{1-u^2}$ as before,

$$\begin{aligned}
&\frac{K_2 e^{j\theta} + K_1 + K_0 e^{-j\theta}}{e^{j\theta} - 1} \\
&= \frac{K_2(-u+jv) + K_1 + K_0(-u-jv)}{(-u+jv) - 1}, \\
&= \frac{-u(K_2+K_0) + K_1 + jv(K_2 - K_0)}{-(u+1) + jv}, \\
&= \frac{\{-u(K_2+K_0) + K_1 + jv(K_2-K_0)\}(u+1+jv)}{\{-(u+1)+jv\}(u+1+jv)}, \\
&= \frac{-(u+1)\{K_2 - K_1 - (1-2u)K_0\} + jv\{K_2 + K_1 - (1+2u)K_0\}}{-(u+1)^2 - (1-u^2)}, \\
&= \frac{1}{2}\{K_2 - K_1 - (1-2u)K_0\} - j\frac{v}{1+u}\frac{1}{2}\{K_2 + K_1 - (1+2u)K_0\} \\
&=: C(u)
\end{aligned} \tag{3.27}$$

Let

$$\begin{aligned}
W_0 &:= \frac{1}{2}K_2 - \frac{1}{2}K_1 \\
W_1 &:= \frac{1}{2}K_2 + \frac{1}{2}K_1.
\end{aligned} \tag{3.28}$$

By substituting (3.28) into (3.27), we obtain

$$C(u) = \left(W_0 - \frac{(1-2u)}{2}K_0\right) - j\frac{v}{(1+u)}\left(W_1 - \frac{(1+2u)}{2}K_0\right). \tag{3.29}$$

Let

$$\tilde{W}_0 := W_0 - \frac{(1-2u)}{2}K_0 \tag{3.30}$$

$$\tilde{W}_1 := W_1 - \frac{(1+2u)}{2}K_0. \tag{3.31}$$

so that (3.19) can be rewritten as follows:

$$|1 + P(u)C(u)|^2 > \frac{1}{\gamma^2} \tag{3.32}$$

$$\Leftrightarrow |1+(R+jvT)(\tilde{W}_0 - j\frac{v}{(1+u)}\tilde{W}_1)|^2 > \frac{1}{\gamma^2} \tag{3.33}$$

$$\Leftrightarrow \left(1+R\tilde{W}_0+\frac{v^2}{(1+u)}T\tilde{W}_1\right)^2 + v^2\left(T\tilde{W}_0 - \frac{1}{(1+u)}R\tilde{W}_1\right)^2 > \frac{1}{\gamma^2} \tag{3.34}$$

$$\Leftrightarrow \Bigg(R^2\tilde{W}_0^2 + \frac{v^4}{(1+u)^2}T^2\tilde{W}_1^2 + 2R\tilde{W}_0 \tag{3.35}$$

$$+\frac{2v^2}{(1+u)}T\tilde{W}_1 + \frac{2v^2}{(1+u)}R\tilde{W}_0T\tilde{W}_1 + 1\Bigg)$$

$$+ v^2\left(T^2\tilde{W}_0^2 + \frac{1}{(1+u)^2}R^2\tilde{W}_1^2 - \frac{2}{(1+u)}T\tilde{W}_0R\tilde{W}_1\right) > \frac{1}{\gamma^2} \tag{3.36}$$

$$\Leftrightarrow \Big(R^2\tilde{W}_0^2 + v^2T^2\tilde{W}_0^2 + 2R\tilde{W}_0 + 1\Big)$$

$$+ v^2\left(\frac{1}{(1+u)^2}R^2\tilde{W}_1^2 + \frac{v^2}{(1+u)^2}T^2\tilde{W}_1^2 + \frac{2}{(1+u)}T\tilde{W}_1\right) > \frac{1}{\gamma^2} \tag{3.37}$$

$$\Leftrightarrow \Big(|P|^2\tilde{W}_0^2 + 2R\tilde{W}_0 + 1\Big)$$

$$+ v^2\left(\frac{1}{(1+u)^2}|P|^2\tilde{W}_1^2 + \frac{2}{(1+u)}T\tilde{W}_1\right) > \frac{1}{\gamma^2} \tag{3.38}$$

$$\Leftrightarrow |P|^2\left(\tilde{W}_0 + \frac{R}{|P|^2}\right)^2 - \frac{R^2}{|P|^2} + 1$$

$$+ v^2|P|^2\left(\frac{1}{(1+u)}\tilde{W}_1 + \frac{T}{|P|^2}\right)^2 - \frac{v^2T}{|P|^2} > \frac{1}{\gamma^2} \tag{3.39}$$

$$\Leftrightarrow |P|^2\left(\tilde{W}_0 + \frac{R}{|P|^2}\right)^2 + \frac{v^2|P|^2}{(1+u)^2}\left(\tilde{W}_1 + \frac{(1+u)T}{|P|^2}\right)^2 > \frac{1}{\gamma^2} \tag{3.40}$$

$$\Leftrightarrow \frac{\left(\tilde{W}_0 + \frac{R}{|P|^2}\right)^2}{1/|P|^2} + \frac{\left(\tilde{W}_1 + \frac{(1+u)T}{|P|^2}\right)^2}{(1+u)^2/v^2|P|^2} > \frac{1}{\gamma^2} \tag{3.41}$$

$$\Leftrightarrow \frac{\left(\tilde{W}_0 + \frac{R}{|P|^2}\right)^2}{\frac{1}{\gamma^2|P|^2}} + \frac{\left(\tilde{W}_1 + \frac{(1+u)T}{|P|^2}\right)^2}{\frac{(1+u)^2}{\gamma^2v^2|P|^2}} > 1 \tag{3.42}$$

$$\Leftrightarrow \frac{\left(W_0 - \frac{(1-2u)}{2}K_0 + \frac{R}{|P|^2}\right)^2}{\frac{1}{\gamma^2|P|^2}} + \frac{\left(W_1 - \frac{(1+2u)}{2}K_0 + \frac{(1+u)T}{|P|^2}\right)^2}{\frac{(1+u)^2}{\gamma^2v^2|P|^2}} > 1 \tag{3.43}$$

$$\Leftrightarrow \frac{\left(W_0 - \frac{(1-2u)}{2}K_0 + \frac{R_P(u)}{|P|^2}\right)^2}{\frac{1}{\gamma^2|P|^2}} + \frac{\left(W_1 - \frac{(1+2u)}{2}K_0 + \frac{(1+u)T_P(u)}{|P|^2}\right)^2}{\frac{(1+u)^2}{\gamma^2v^2|P|^2}} > 1. \tag{3.44}$$

For a fixed $K_0 = K_0^*$, (3.44) represents the exterior of an axis-parallel ellipse $F_\gamma(u, K_0^*)$ in (W_0, W_1) space for each $u \in (-1, 1)$. Using the mapping in (3.28), we obtain the ellipse $E_\gamma(u, K_0^*)$

in (K_1, K_2) space for each $u \in (-1, 1)$.

Denoting $\mathcal{S}(K_0^*)$ by the stabilizing set of $\mathcal{S}$ for a fixed $K_0 = K_0^*$, we define a subset of $\mathcal{S}(K_0^*)$ as follows:

$$\mathcal{S}_\gamma(u, K_0^*) := \mathcal{S}(K_0^*) \setminus E_\gamma^o(u, K_0^*), \ \forall\, u \ \in \ (-1, 1).$$

By Theorem 3.1, it is easy to see that

$$\mathcal{S}_\gamma(K_0^*) = \bigcap_{u \in (-1,1)} \mathcal{S}_\gamma(u, K_0^*).$$

Finally, we can obtain $\mathcal{S}_\gamma$ by sweeping K_0 over the range for which $\mathcal{S}(K_0)$ is nonempty:

$$\mathcal{S}_\gamma = \bigcup_{K_0} \mathcal{S}_\gamma(K_0).$$

3.4 Examples

We present four numerical examples which illustrate our approach.

Example 3.4. Consider the second order plant and the PI controller:

$$P(z) = \frac{0.5}{z^2 - z + 0.5}, \ \ C(z) = \frac{K_1 z + K_0}{z - 1}. \tag{3.45}$$

The stabilizing set is first computed for the plant and the PI controller given in (3.45). Fig. 3.4 shows the stabilizing set (yellow) in (K_0, K_1) space. The stabilizing set is mapped to (L_0, L_1) space in order to compute $\mathcal{S}_\gamma$ sets for $\gamma = 1.6$, 2.0 and 4.0 in Fig. 3.3. Then, the $\mathcal{S}_\gamma$ sets in (L_0, L_1) space given by (3.21) are mapped back to (K_0, K_1) space to obtain the PI controllers achieving the H_∞ norm $< \gamma$ specification as shown in Fig. 3.4.

Fixing $\gamma = 2$, some of the boundary points of the $\mathcal{S}_\gamma$ set are chosen for displaying the Nyquist plots. It is important to verify that the Nyquist plots stay outside of a circle centered at the critical point $-1 + j0$ with radius of $1/\gamma$. In Fig. 3.5, the Nyquist plots are at least 0.5 away from the critical point.

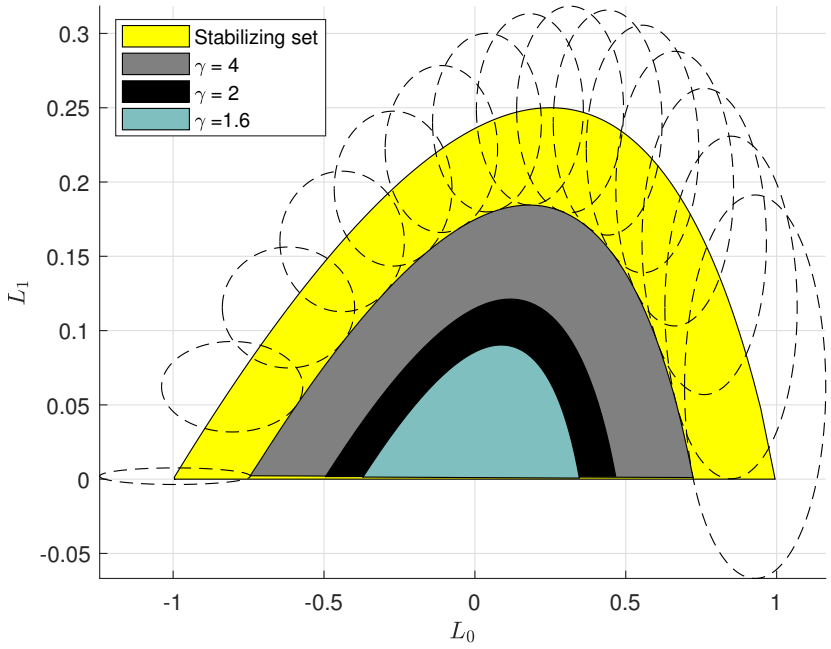

Figure 3.3: $\mathcal{S}_\gamma$ for $\gamma = 1.6$, 2.0 and 4.0 with the stabilizing set in (L_0, L_1) space.

Example 3.5. Consider the second order plant and the PI controller:

$$\begin{aligned} P(z) &= \frac{0.522z + 0.4529}{z^2 + 0.215z + 0.2422}, \\ C(z) &= \frac{K_1 z + K_0}{z - 1}. \end{aligned} \tag{3.46}$$

The plant $P(z)$ is a discrete time model of a lathe process in [10]. We compute $\mathcal{S}$ in (K_0, K_1) space and map the set into (L_0, L_1) space using the map W in (3.16). Since an axis parallel ellipse can be drawn in (L_0, L_1) from (3.21) for a fixed $u \in (-1, 1)$, we fix $\gamma > 0$ and calculate the family of ellipses by sweeping u over the range $(-1, 1)$. The set $\mathcal{S}_\gamma$ for a prescribed γ in (L_0, L_1) space is then obtained by intersecting the outside of the family of the ellipses with the stabilizing set $\mathcal{S}$.

The $\mathcal{S}_\gamma$ sets for various γ values are shown in Fig. 3.6 and Fig. 3.7. For $\gamma = 4$, the family of ellipses are overlapped with $\mathcal{S}$ in order to depict the graphical determination of $\mathcal{S}_\gamma$ sets. It can be observed that the sets $\mathcal{S}_\gamma$ are telescoping as γ decreases (Fact 3.2.)

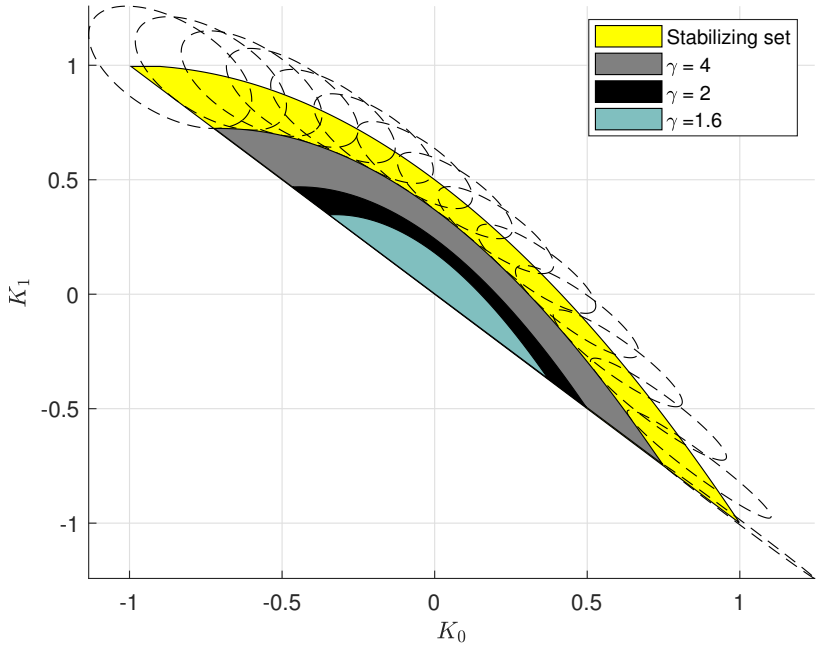

Figure 3.4: $\mathcal{S}_\gamma$ for $\gamma = 1.6$, 2.0 and 4.0 with the stabilizing set in (K_0, K_1) space.

For $\gamma = 2$, the Nyquist plots of the plant $P(z)$ and some of digital PI controllers $C(z)$ in the $\mathcal{S}_\gamma$ set are displayed. As expected, the Nyquist plots stay outside of a circle centered at the critical point $-1 + j0$ with radius of $1/\gamma$. In Fig. 3.8, the Nyquist plots are at least 0.5 away from the critical point.

Example 3.6. Consider the second order plant and the PID controller:

$$P(z) = \frac{1}{z^2 - 0.25}, \quad C(z) = \frac{K_2 z^2 + K_1 z + K_0}{z(z-1)}. \tag{3.47}$$

The stabilizing set $\mathcal{S}$ is computed for the plant $P(z)$ and the PID controller $C(z)$ in (3.47). Fig. 3.9 shows $\mathcal{S}$ in (K_0, K_1, K_2) space. We fix $\gamma = 2$ and $\mathcal{S}_\gamma$ is overlapped with $\mathcal{S}$.

Fix $K_0 = -0.1$. In (W_0, W_1) space, the H_∞ criterion in (3.19) is represented by the outside of an axis-parallel ellipse for a fixed u. Since the criterion is the worst case condition — the

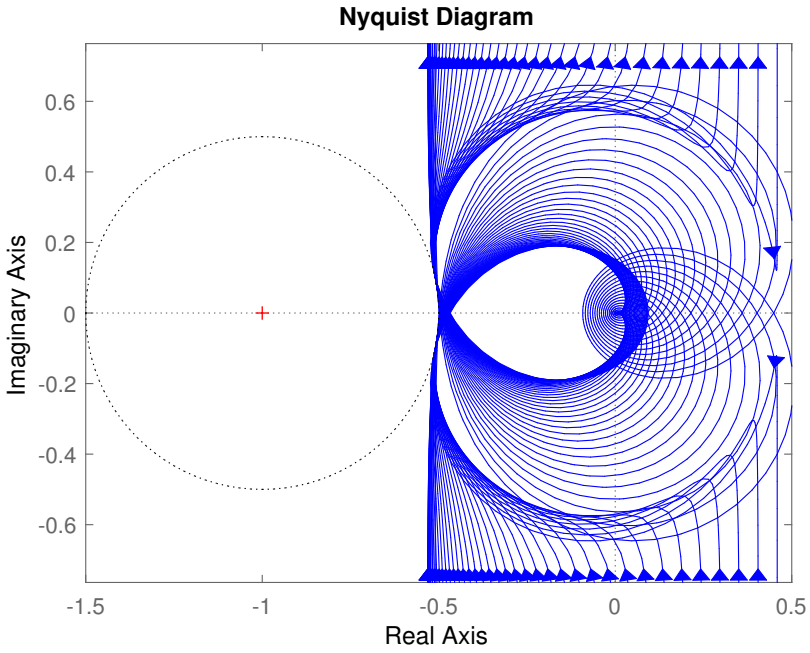

Figure 3.5: Nyquist plots with (K_0, K_1) along the boundary curve of $\mathcal{S}_\gamma$ with $\gamma = 2$.

maximum magnitude is less than γ, the family of ellipses is drawn and the intersection of all outsides of ellipses is the admissible region. The family of ellipses are drawn in Fig. 3.10. $\mathcal{S}_\gamma$ in (W_0, W_1) space is thus the intersection of $\mathcal{S}(K_0 = -0.1)$ and the outside of ellipses.

Now we map the set $\mathcal{S}_\gamma$ in (W_0, W_1) space to (K_1, K_2) space for $K_0 = -0.1$. Sweeping over K_0 gives the set $\mathcal{S}_\gamma$ as seen in Fig. 3.9. Since the mapping in (3.28) is not a diagonal matrix, each mapped ellipse is not necessarily an axis-parallel ellipse. In Fig. 3.11, the family of ellipses is displayed and overlapped with the stabilizing set $\mathcal{S}_\gamma(K_0)$.

Example 3.7. Consider the second order plant and the PID controller:

$$\begin{aligned} P(z) &= \frac{-0.009652z + 0.01015}{z^2 - 1.98z + 0.9802}, \\ C(z) &= \frac{K_2 z^2 + K_1 z + K_0}{z(z-1)}. \end{aligned} \tag{3.48}$$

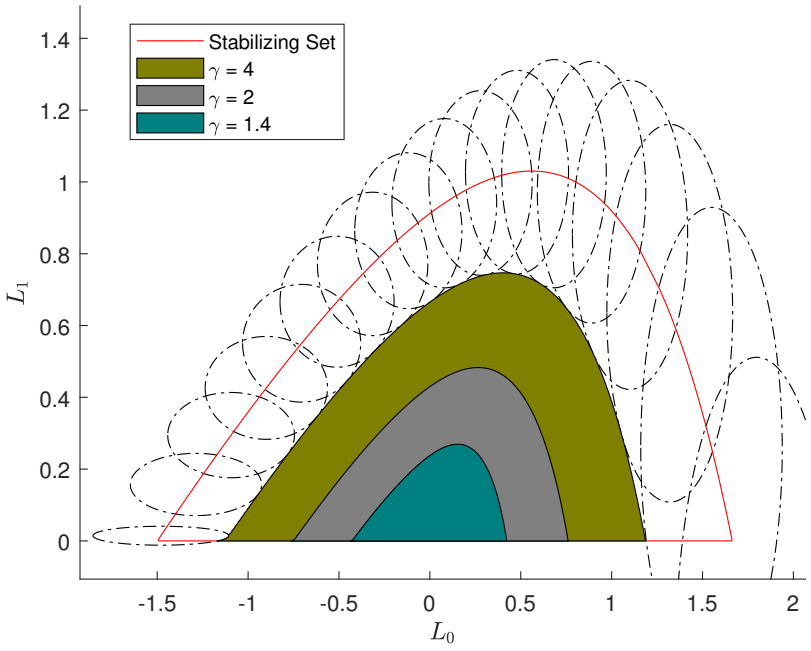

Figure 3.6: $\mathcal{S}_\gamma$ for $\gamma = 1.4$, 2.0 and 4.0 with the stabilizing set in (L_0, L_1) space.

The plant $P(z)$ in (3.48) is a discretized model of

$$P(s) = \frac{-s+5}{(s+1)^2}. \tag{3.49}$$

In [8], the same plant was used and the result of loop-shaping optimization was the controller:

$$C_{ref}(z) = \frac{1.0156z^2 - 1.864942z + 0.85}{z(z-1)}. \tag{3.50}$$

This controller renders the H_∞ norm of the error transfer function less than $\gamma = 1.236$. Since $K_0 = 0.85$ in (3.50), we can fix K_0 to 0.85 and compute $\mathcal{S}(K_0 = 0.85)$ as shown in Fig. 3.12.

It is observed, however, that the set $\mathcal{S}(K_0 = 0.85)$ is difficult to be further exploited in (K_1, K_2) space because the set is nearly a line segment tilted by 45^o. Thus, we map the set into (W_0, W_1) space and it is shown in Fig. 3.13.

In (W_0, W_1) space, the $\mathcal{S}_\gamma$ sets for various γ values are drawn. (Fig. 3.13) In particular, $\mathcal{S}_\gamma$

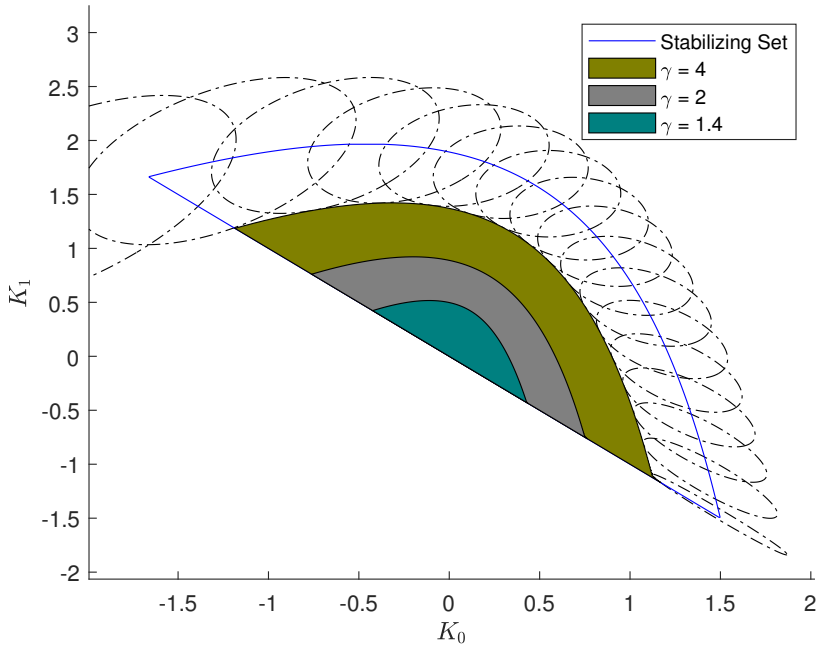

Figure 3.7: $\mathcal{S}_\gamma$ for $\gamma = 1.4$, 2.0 and 4.0 with the stabilizing set in (K_0, K_1) space.

with $\gamma = 1.236$ is identified much better than in (K_1, K_2) space. Following the approach we discussed earlier, we see that the entire set $\mathcal{S}_\gamma$ with $\gamma = 1.236$ and $K_0 = 0.85$ can be constructively determined as shown in Fig. 3.13. Moreover, as γ decreases, γ^* is numerically determined to be $\gamma^* = 1.01$ (Remark 3.3.)

Now, we verify that the set $\mathcal{S}_\gamma$ achieves the H_∞ norm less than $\gamma = 1.236$. The Nyquist plots for the set are shown in Fig. 3.14. It is seen that the controllers $C(z)$ in $\mathcal{S}_\gamma$ with $\gamma = 1.236$ renders the Nyquist plots of the open loop transfer function $P(z)C(z)$ to stay outside the circle at $-1 + j0$ with radious $1/\gamma$.

For controller synthesis, one should also consider time response specifications such as overshoot and settling time. In [8], the controller $C_{ref}(z)$ in (3.50) gives 0% overshoot and 13.8 seconds of setting time. We chose three sample controllers in Table 3.1 from $\mathcal{S}_\gamma$ with $\gamma = 1.236$ and plotted the step responses in Fig. 3.15.

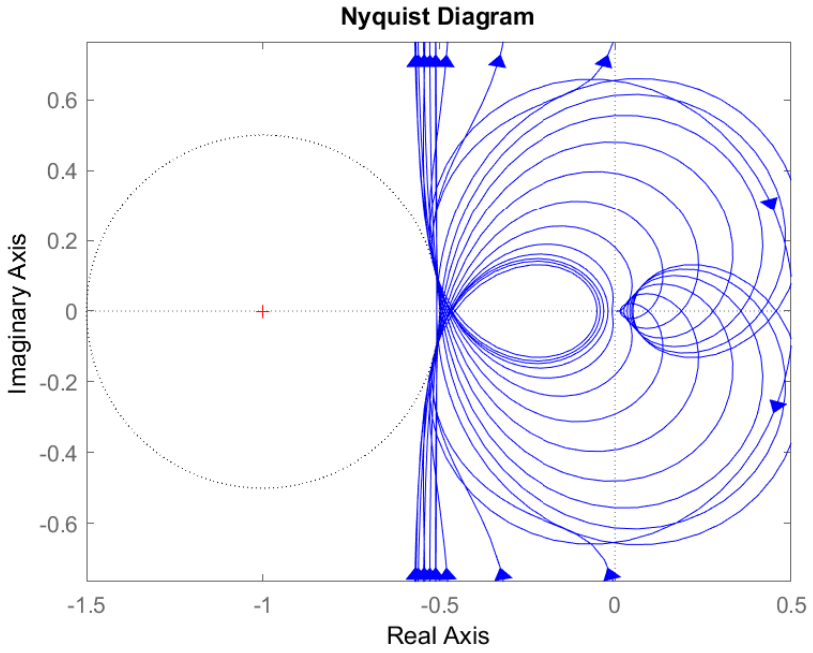

Figure 3.8: Nyquist plots of $P(z)C(z)$ in (3.46) along the curve of $\gamma = 2$.

Table 3.1: Overshoot (OS) and settling time (ST) for various controllers in $\mathcal{S}_\gamma$ set.

	K_2	K_1	K_0	OS (%)	ST (sec.)
$C_1(z)$	0.9123	-1.7616	0.85	1.2	7.44
$C_2(z)$	0.9558	-1.8050	0.85	0.0	6.68
$C_3(z)$	0.9899	-1.8392	0.85	0.0	9.90
$C_{ref}(z)$	1.0156	- 1.8649	0.85	0.0	13.76
$C(z)$ in $\mathcal{S}_{\gamma^*}$	0.8674	-1.7173	0.85	0.0	83.79

3.5 Notes and References

In [11], Ho proposed an H_∞ approach using a generalization of Hermite-Biehler theorem for complex polynomials. Gryazina et al. [12] represented the H_∞ criterion by a family of ellipses in the controller parameter space and Han et al. [4] presented a method which superimposed the family of ellipses over the stabilizing set. These methods were developed for continuous time systems.

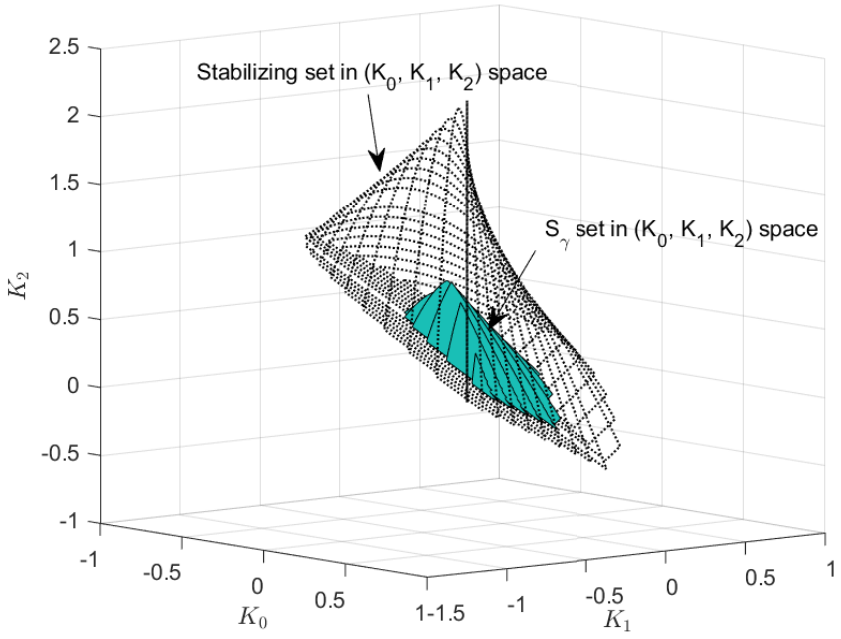

Figure 3.9: The stabilizing set in (K_0, K_1, K_2) space.

There are other PID controller tuning methods achieving robustness of the system, such as loop-shaping [13, 8], auto-tuning and neural networks [14, 15, 16, 17], particle swarm optimization [18] dominant pole placement [19] and linear matrix inequality (LMI) [20, 21].

Digital PID controllers are used in many applications such as DC-DC converters [22, 23], underwater robots [24], lathe machine [10], bitumen tank [25] and unmanned aerial vehicles [26].

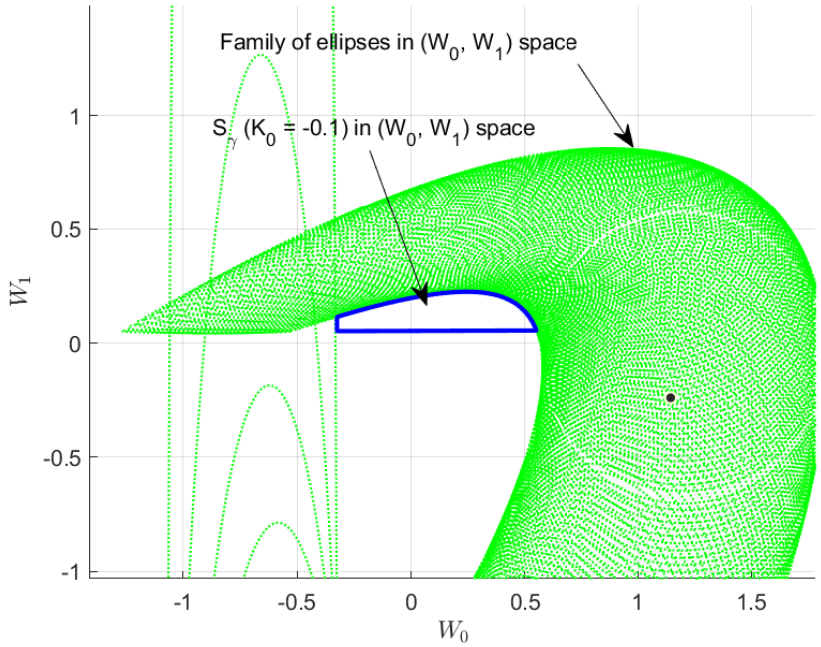

Figure 3.10: The family of axis-parallel ellipses in (W_0, W_1) space as u runs from -1 to 1.

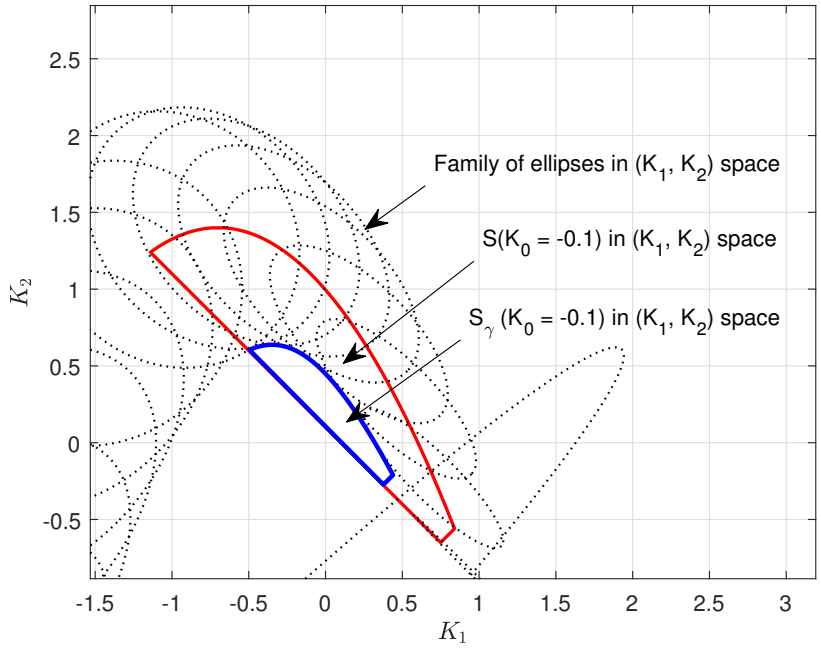

Figure 3.11: $\mathcal{S}_\gamma(K_0)$ and the family of ellipses in (K_1, K_2) space with $K_0 = -0.1$.

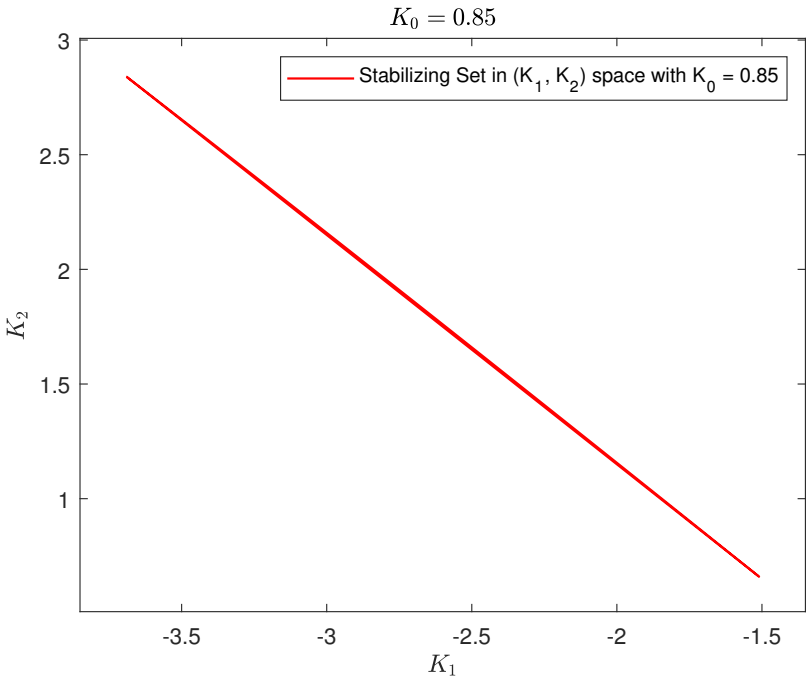

Figure 3.12: $\mathcal{S}(K_0 = 0.85)$.

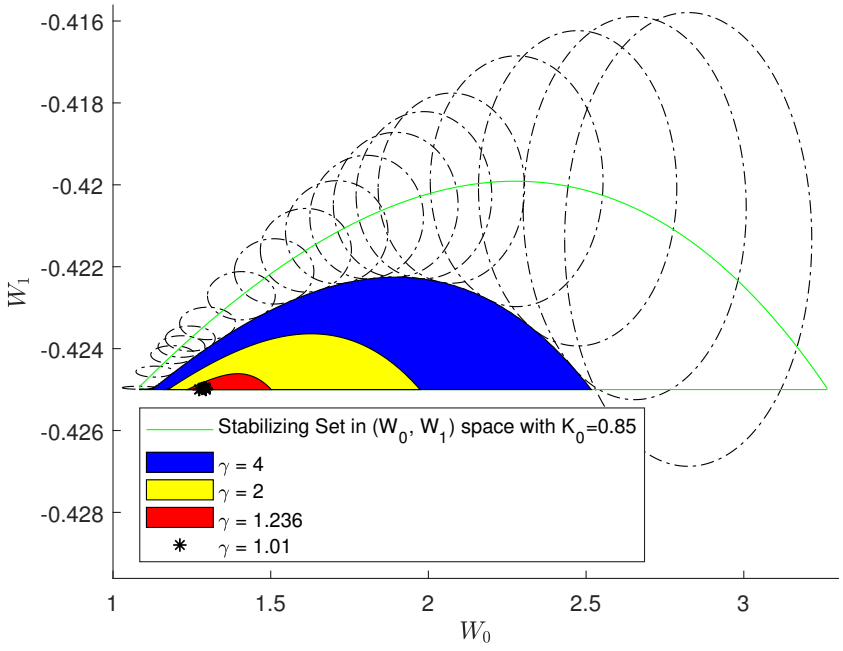

Figure 3.13: $\mathcal{S}(K_0 = 0.85)$ and $\mathcal{S}_\gamma$ sets for various γ values in (W_0, W_1) space. The family of axis-parallel ellipses $E_\gamma(u, K_2, K_1, K_0 = 0.85)$ as u runs from -1 to 1 is overlapped to illustrate the procedure.

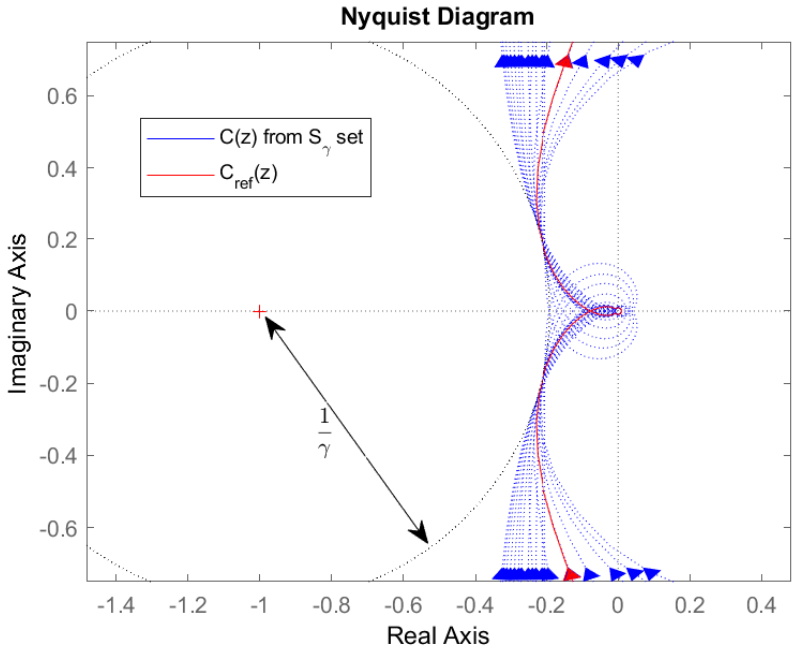

Figure 3.14: Nyquist plots for $P(z)$ and $C(z)$ from $\mathcal{S}_\gamma$ with $\gamma = 1.236$.

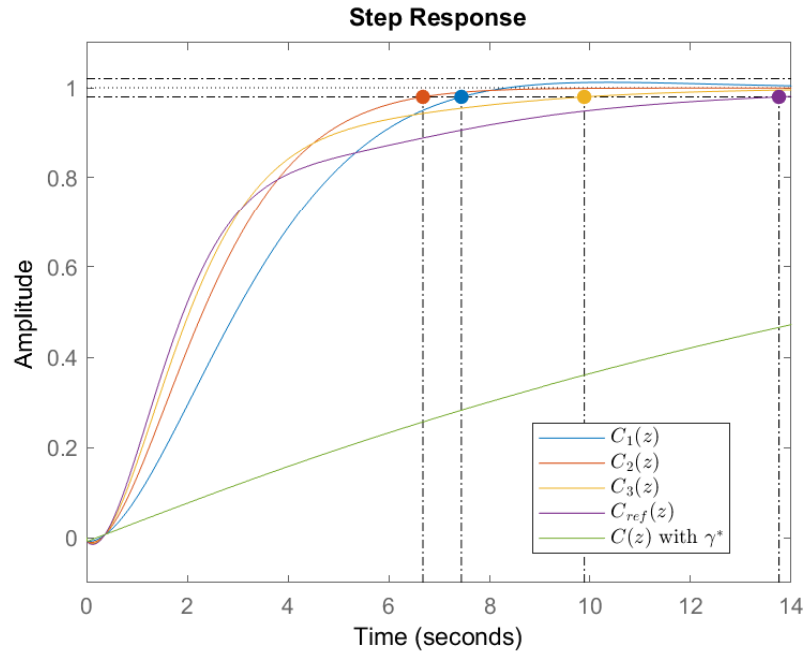

Figure 3.15: Step responses for $C(z)$ from Table 3.1 and $C_{ref}(z)$. The solid dots indicate the settling times. '$C(z)$ with γ^*' is the controller $C(z)$ in $\mathcal{S}_{\gamma^*}$ with $\gamma^* = 1.01$.

4. σ-HURWITZ STABILITY *

In some applications, it may be necessary to push the closed-loop characteristic roots to the left of a line $s = -\sigma$ to speed up the time response. In this chapter, we present a constructive determination of $\mathcal{S}(\sigma)$, the subset of $\mathcal{S}$ for which the closed loop poles have real parts less than $-\sigma$. By this means, we can also determine the maximum achievable σ for a given plant. It is simply the smallest σ for which $\mathcal{S}(\sigma) = \varnothing$.

4.1 Introduction

The performance of a Linear Time Invariant (LTI) control system is dependent on the location of the closed loop poles. When the step response converges the decay rate is determined by the poles that are closest to the imaginary axis. Thus, the settling time of the step response is inversely proportional to the distance of the closest poles from the imaginary axis.

Recently, the computation of a set of all stabilizing PI/PID controllers has been reported in [3] and the set is called the *stabilizing set* $\mathcal{S}$. The main contribution of the proposed method in this paper is the constructive determination of $\mathcal{S}(\sigma)$, the subset of $\mathcal{S}$ for which the closed loop poles have real parts less than $-\sigma$. By this means, we can also determine the maximum achievable σ for a given plant. Although it is a straightforward extension of the 'signature method' in [3] to σ-Hurwitz stability, the proposed method is an important hitherto unsolved problem.

4.2 σ-Hurwitz Stability

Consider a monic polynomial $\delta(s)$ of degree n with real coefficients. Write

$$\delta(s) = (s - \lambda_1) \cdots (s - \lambda_n) \tag{4.1}$$

where $\lambda_i \in \mathbb{C}, \forall i \in \{1, \ldots, n\}$.

Definition 4.1. For $\sigma \geq 0$, $\delta(s)$ is *σ-Hurwitz* stable if all its roots have real part less than $-\sigma$, that

*Sections 4.1, 4.2, 4.3 and 4.4 are reprinted from Sangjin Han, S. P. Bhattacharyya *PID Controller Synthesis Using a σ-Hurwitz Stability Criterion. IEEE Control Systems Letters,* with permission © 2018 IEEE.

is, $\text{Re}\{\lambda_i\} < -\sigma \ \forall i$.

Define s' such that $s = s' - \sigma$ and $\delta'(s') := \delta(s' - \sigma)$. Then we have the following fact.

Fact 4.2. $\delta'(s')$ is Hurwitz if and only if $\delta(s)$ is σ-Hurwitz.

Remark 4.3. A Hurwitz polynomial is a special case of a σ-Hurwitz polynomial with $\sigma = 0$.

4.3 σ-Hurwitz PID Stabilizing Set

4.3.1 Problem Formulation

Consider a unity feedback loop with a PID controller and a plant in Fig. 4.1, where

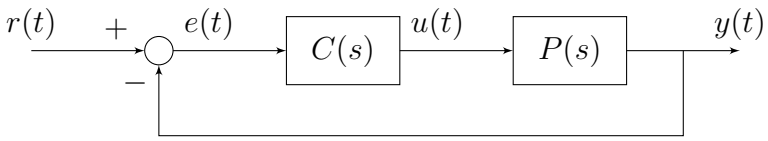

Figure 4.1: Unity feedback control loop.

$$P(s) = \frac{N(s)}{D(s)}, \tag{4.2}$$

$$C(s) = k_p + \frac{k_i}{s} + k_d s. \tag{4.3}$$

Let

$$\mathcal{S}(\sigma) := \{(k_p, k_i, k_d) \colon \delta(s, k_p, k_i, k_d) \text{ is } \sigma\text{-Hurwitz}\} \tag{4.4}$$

denote the set of PID controllers that stabilize $P(s)$ for which the characteristic polynomial $\delta(s, k_p, k_i, k_d)$ is σ-Hurwitz.

Fact 4.4. If $0 \leq \sigma_1 \leq \sigma_2$, then $\mathcal{S}(\sigma_1) \supseteq \mathcal{S}(\sigma_2)$.

We find below $\mathcal{S}(\sigma)$ for a prescribed σ. Moreover, we constructively determine the maximum achievable $\sigma < \infty$ for which $\mathcal{S}(\sigma)$ just becomes empty.

4.3.2 Signature Method for σ-Hurwitz polynomials

In order for $\delta(s)$ to be σ-Hurwitz, we examine whether or not $\delta'(s')$ is Hurwitz using Fact 4.2. Observe that

$$\delta'(s') = \delta(s' - \sigma) \tag{4.5}$$

$$= (s' - \sigma) \underbrace{D(s' - \sigma)}_{=:D'(s')} + (k_i + k_p(s' - \sigma) + k_d(s' - \sigma)^2) \underbrace{N(s' - \sigma)}_{=:N'(s')}. \tag{4.6}$$

Define $N'_{\text{even}}(s'^2)$, $N'_{\text{odd}}(s'^2)$, $D'_{\text{even}}(s'^2)$ and $D'_{\text{odd}}(s'^2)$ through

$$N'(s') = N'_{\text{even}}(s'^2) + s' N'_{\text{odd}}(s'^2), \tag{4.7}$$

$$D'(s') = D'_{\text{even}}(s'^2) + s' D'_{\text{odd}}(s'^2). \tag{4.8}$$

Then,

$$N'(-s') = N'_{\text{even}}(s'^2) - s' N'_{\text{odd}}(s'^2). \tag{4.9}$$

Let $\mathbb{C}_\sigma^-$ denote the open half plane to the left of the line $\text{Re}\{s\} = -\sigma$, $\mathbb{C}_\sigma^+$ the closed half plane to the right of $\text{Re}\{s\} = -\sigma$, and z_σ^- and z_σ^+ the numbers of roots of $N'(s')$ in $\mathbb{C}_\sigma^-$ and $\mathbb{C}_\sigma^+$, respectively. Then, $N'(-s')$ has z_σ^+ roots in $\mathbb{C}_\sigma^-$ and z_σ^- roots in $\mathbb{C}_\sigma^+$.

Assume $N(s)$ has no roots on $\text{Re}\{s\} = -\sigma$. Consider the net change in the phase of $N(s)|_{s=-\sigma+j\omega}$ from $\omega = 0$ to $\omega = \infty$. This is equivalent to the net change in the phase of $N'(s')|_{s'=j\omega}$ and

$$\Delta_{\omega=0}^{\infty} \angle N'(j\omega) = \frac{\pi}{2}(z_\sigma^- - z_\sigma^+). \tag{4.10}$$

We call $z_\sigma^- - z_\sigma^+$ the *σ-signature* of $N'(s')$ and denote it as

$$\sigma\text{-signature}(N') := z_\sigma^- - z_\sigma^+. \tag{4.11}$$

We form the new polynomial

$$\nu'(s') := \delta'(s')N'(-s') \tag{4.12}$$

and state the condition for σ-Hurwitz stability of the closed loop system in terms of $\nu'(s')$ in the following.

Theorem 4.5. *The closed loop system is σ-Hurwitz stable if and only if*

$$\sigma\text{-}\textit{signature}(\nu') = n + 1 - m + 2z_\sigma^+. \tag{4.13}$$

Proof. By Fact 4.2, it suffices to show that $\delta'(s')$ is Hurwitz stable. This is equivalent to

$$\begin{aligned} \sigma\text{-signature}(\nu') &= n + 1 - z_\sigma^- + z_\sigma^+ \\ &= n + 1 - m + 2z_\sigma^+. \end{aligned}$$

□

We substitute (4.7), (4.8) and (4.9) into (4.12), to get

$$\begin{aligned} \nu'(s') &= \delta'(s')N'(-s') \\ &= Q_0(s') + (k_2 + k_3 s'^2)Q_1(s') + k_1 s' Q_1(s') \end{aligned} \tag{4.14}$$

where

$$\begin{aligned} Q_0(s') &= (s' - \sigma)(D'_{\text{even}}(s') + s'D'_{\text{odd}}(s'))(N'_{\text{even}}(s') - s'N'_{\text{odd}}(s')), \\ Q_1(s') &= N'^2_{\text{even}}(s') - s'^2 N'^2_{\text{odd}}(s'), \end{aligned}$$

$$k_1 = k_p - 2\sigma k_d, \;\; k_2 = -\sigma k_p + k_i + \sigma^2 k_d, \;\; k_3 = k_d.$$

It is easy to see that the transformation from k_p, k_i, k_d to k_1, k_2, k_3 is a linear map and is

invertible for all σ. We have

$$\begin{bmatrix} k_p \\ k_i \\ k_d \end{bmatrix} = \begin{bmatrix} 1 & 0 & 2\sigma \\ \sigma & 1 & \sigma^2 \\ 0 & 0 & 1 \end{bmatrix} \begin{bmatrix} k_1 \\ k_2 \\ k_3 \end{bmatrix}. \tag{4.15}$$

We can see that $\nu'(s')$ exhibits the parameter separation property in terms of k_1, k_2, k_3 just as $\nu(s)$ does with respect to k_p, k_i, k_d.

By fixing $k_1 = k_1^*$, we can determine the zeros of the imaginary part of $\nu'(j\omega)$. There exist sets of linear inequalities in terms of k_2 and k_3 for such fixed k_1^*. By intersecting the half planes from the inequalities in each set, we find the stabilizing set in (k_2, k_3) space. By sweeping over different k_1 values we obtain the stabilizing set in (k_1, k_2, k_3) space. By the transformation in (4.15), we obtain $\mathcal{S}(\sigma)$ in (k_p, k_i, k_d) space for a prescribed σ. The maximum achievable σ can be found by increasing σ until $\mathcal{S}(\sigma)$ just becomes empty.

4.4 Examples – Computation of achievable σ

The constructive procedure of the algorithm that finds $\mathcal{S}(\sigma)$, the subset of the stabilizing set $\mathcal{S}$ for a prescribed σ is demonstrated by three examples.

Example 4.6. Consider the plant and controller:

$$P(s) = \frac{s-2}{s^2+4s+3}, \;\; C(s) = k_p + \frac{k_i}{s}. \tag{4.16}$$

Substitute (4.16) into (4.6). Since

$$N(s) = s - 2, \;\; D(s) = s^2 + 4s + 3,$$

we have

$$N'(s') = s' - \sigma - 2, \tag{4.17}$$

$$N'_{\text{even}}(s'^2) = -\sigma - 2, \tag{4.18}$$

$$N'_{\text{odd}}(s'^2) = 1, \tag{4.19}$$

and

$$\begin{aligned} D'(s') &= (s'-\sigma)^2 + 4(s'-\sigma) + 3, \\ &= s'^2 + (4-2\sigma)s' + \sigma^2 - 4\sigma + 3, \end{aligned} \tag{4.20}$$

$$D'_{\text{even}}(s'^2) = s'^2 + \sigma^2 - 4\sigma + 3, \tag{4.21}$$

$$D'_{\text{odd}}(s'^2) = -2\sigma + 4. \tag{4.22}$$

Substituting $N'_{\text{even}}(s'^2)$, $N'_{\text{odd}}(s'^2)$, $D'_{\text{even}}(s'^2)$ and $D'_{\text{odd}}(s'^2)$ into (4.14) and evaluating $\nu'(s')$ at $s' = j\omega$, we get

$$\nu'(j\omega) = p(\omega, \sigma, k_2) + jq(\omega, \sigma, k_1) \tag{4.23}$$

where

$$p(\omega, \sigma, k_2) = p_1(\omega, \sigma) + k_2 p_2(\omega, \sigma), \tag{4.24}$$

$$q(\omega, \sigma, k_1) = q_1(\omega, \sigma) + k_1 q_2(\omega, \sigma), \tag{4.25}$$

and

$$\begin{aligned} p_1(\omega, \sigma) &= -\omega^4 + (11 - 10\sigma)\omega^2 + (\sigma^4 - 2\sigma^3 - 5\sigma^2 + 6\sigma), \\ p_2(\omega, \sigma) &= \omega^2 + \sigma^2 + 4\sigma + 4, \\ q_1(\omega, \sigma) &= (6 - 2\sigma)\omega^3 - (2\sigma^3 + 2\sigma^2 - 16\sigma + 6)\omega, \\ q_2(\omega, \sigma) &= \omega\left[\omega^2 + \sigma^2 + 4\sigma + 4\right]. \end{aligned}$$

Suppose we fix $\sigma = 0.5$. Then, by Theorem 4.5, we need for σ-Hurwitz stability

$$\sigma\text{-signature}(\nu') = n + 1 - m + 2z_\sigma^+ \tag{4.26}$$

$$= 2 + 1 - 1 + 2 \cdot 1 \tag{4.27}$$

$$= 4. \tag{4.28}$$

The admissible range for k_1 is such that $q(\omega, \sigma = 0.5, k_1)$ must have at least 1 positive zero with odd multiplicity. This was graphically determined to be $(-5, -0.2)$.

For a fixed $k_1 \in (-5, -0.2)$, for instance, $k_1 = -1$, we have

$$q(\omega, \sigma = 0.5, k_1 = -1) = 4\omega^3 - 5\omega \tag{4.29}$$

and the nonnegative distinct zeros of $q(\omega, \sigma = 0.5, k_1 = -1)$ with odd multiplicities are

$$\omega_0 = 0,\ \omega_1 = \frac{\sqrt{5}}{2}. \tag{4.30}$$

We also define $\omega_2 := \infty$. Since

$$\text{sgn}[q(0^+, 0.5, -1)] = -1,$$

it follows that the stabilizing k_2 values corresponding to $k_1 = -1$ must satisfy the string of inequalities:

$$p_1(\omega_0, \sigma = 0.5) + k_2 p_2(\omega_0, \sigma = 0.5) < 0, \tag{4.31}$$

$$p_1(\omega_1, \sigma = 0.5) + k_2 p_2(\omega_1, \sigma = 0.5) > 0, \tag{4.32}$$

$$p_1(\omega_2, \sigma = 0.5) + k_2 p_2(\omega_2, \sigma = 0.5) < 0. \tag{4.33}$$

Substituting for ω_0, ω_1 and ω_2, we have

$$1.5625 + 6.25k_2 < 0, \tag{4.34}$$

$$7.499 + 7.499k_2 > 0, \tag{4.35}$$

and this yields $-1 < k_2 < -0.25$.

Using (4.15), the line segment in (k_1, k_2) space

$$\{(k_1, k_2) : k_1 = -1, -1 < k_2 < -0.25\} \tag{4.36}$$

is mapped back to the line segment in (k_p, k_i) space

$$\{(k_p, k_i) : k_p = -1, -1.5 < k_i < -0.75\}\,. \tag{4.37}$$

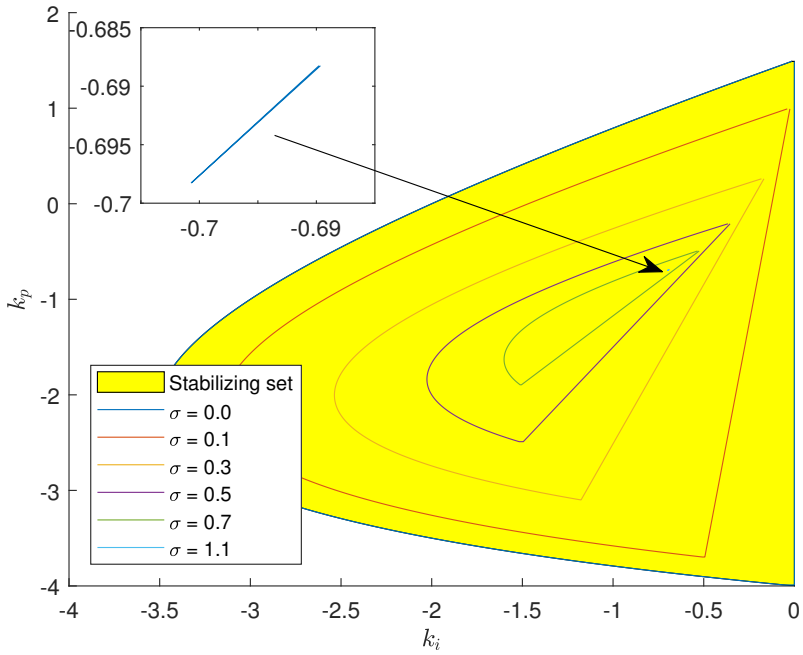

Figure 4.2: $\mathcal{S}(\sigma)$ sets for various σ values. © 2018 IEEE

By sweeping over different k_1 values within the interval $(-5, -0.2)$ and repeating the procedure, we get the stabilizing set in (k_1, k_2) space and finally mapping the set back to (k_p, k_i) space we get $\mathcal{S}(\sigma)$ for $\sigma = 0.5$.

The sets $\mathcal{S}(\sigma)$ are displayed for different σ values in Fig. 4.2. The set colored in yellow is the

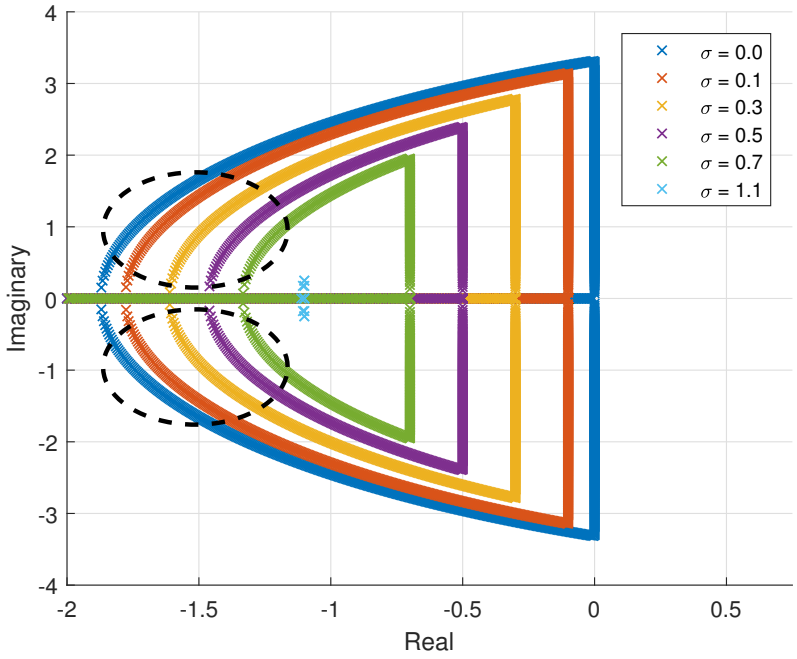

Figure 4.3: The closed loop poles for various σ values. © 2018 IEEE

Hurwitz stabilizing set and it is consistent with $\mathcal{S}(\sigma)$ when $\sigma = 0$. Observe that the sets, $\mathcal{S}(\sigma)$, are telescoping as σ increases, which is consistent with Fact 4.4. It vanishes at around $\sigma = 1.1$. Thus, the maximum achievable σ can be determined to be approximately 1.1.

In order to demonstrate the movement of the closed loop poles, the controllers are selected from the boundary points in the $\mathcal{S}(\sigma)$ sets for different σ values and the closed loop poles are depicted in Fig. 4.3. It is clear that the poles are pushed to the left as σ increases. The closed loop poles appear to be telescoping similar to the $\mathcal{S}(\sigma)$ sets in this example.

Since the plant is of second order and the controller is first order, the resulting closed loop system has three poles. Some complex conjugate poles appear to be pushed more than the prescribed σ, as marked in dashed ellipses in Fig. 4.3, but the third root is located at $s = -\sigma$. It should be noted that the complex conjugate poles are not the rightmost poles but the real root at $s = -\sigma$ is the rightmost pole.

Location of the closed loop poles for several PI controllers and the corresponding step re-

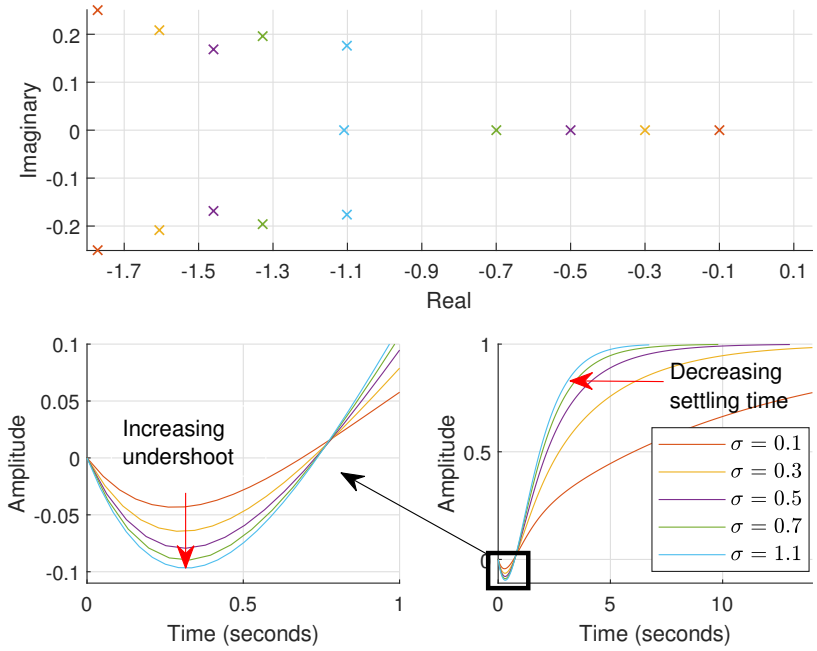

Figure 4.4: Closed loop poles (top) and step responses (bottom) for σ values. © 2018 IEEE

sponses are plotted in Fig. 4.4. We chose PI gains so that each closed loop system had a pair of complex poles whose imaginary part was around 0.2. Observe that settling time decreases as σ increases as expected but undershoot also increases. The closed loop poles are lined up on the line $\text{Re}\{s\} = -\sigma$ when $\sigma = 1.1$.

Example 4.7. Consider the plant and the controller:

$$P(s) = \frac{N(s)}{D(s)}, \quad C(s) = k_p + \frac{k_i}{s} + k_d s, \tag{4.38}$$

where

$$N(s) = s^3 - 2s^2 - s - 1, \tag{4.39}$$

$$D(s) = s^6 + 2s^5 + 32s^4 + 26s^3 + 65s^2 - 8s + 1. \tag{4.40}$$

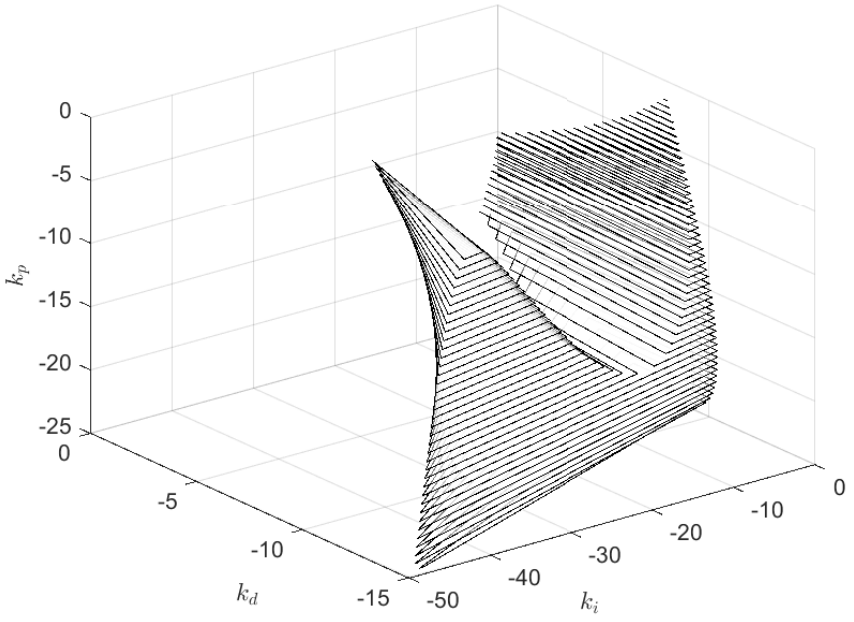

Figure 4.5: $\mathcal{S}(\sigma)$ set for $\sigma = 0$. © 2018 IEEE

From (4.39) and (4.40), we have

$$
\begin{aligned}
N'_{\text{even}}(s'^2) =& -3\sigma s'^2 - \sigma^3 - 2\sigma^2 + \sigma - 1, \\
N'_{\text{odd}}(s'^2) =& s'^2 + 3\sigma^2 + 4\sigma - 1, \\
D'_{\text{even}}(s'^2) =& s'^6 + (15\sigma^2 - 10\sigma + 32)s'^4 + (15\sigma^4 - 20\sigma^3 + 192\sigma^2 - 78\sigma + 65)s'^2 \\
&+ \sigma^6 - 2\sigma^5 + 32\sigma^4 - 26\sigma^3 + 65\sigma^2 + 8\sigma + 1, \\
D'_{\text{odd}}(s'^2) =& (2 - 6\sigma)s'^4 - (20\sigma^3 - 20\sigma^2 + 128\sigma - 26)s'^2 \\
&- 6\sigma^5 + 10\sigma^4 - 128\sigma^3 + 78\sigma^2 - 130\sigma - 8.
\end{aligned}
$$

Substituting the above equations into (4.14) and evaluating $\nu'(s')$ at $s' = j\omega$, we get

$$\nu'(j\omega) = p(\omega, \sigma, k_2, k_3) + jq(\omega, \sigma, k_1) \tag{4.41}$$

where

$$p(\omega, \sigma, k_2, k_3) = p_1(\omega, \sigma) + (k_2 - \omega^2 k_3) p_2(\omega, \sigma)$$

$$q(\omega, \sigma, k_1) = q_1(\omega, \sigma) + k_1 q_2(\omega, \sigma)$$

and

$$\begin{aligned}
p_1(\omega, \sigma) =& N'_{\text{odd}}(-\omega^2)(D'_{\text{even}}(-\omega^2) - \sigma D'_{\text{odd}}(-\omega^2))\omega^2 - D'_{\text{odd}}(-\omega^2)N'_{\text{even}}(-\omega^2)\omega^2 \\
& - \sigma D'_{\text{even}}(-\omega^2)N'_{\text{even}}(-\omega^2), \\
p_2(\omega, \sigma) =& \{N'_{\text{odd}}(-\omega^2)\}^2\omega^2 + \{N'_{\text{even}}(-\omega^2)\}^2, \\
q_1(\omega, \sigma) =& D'_{\text{odd}}(-\omega^2)N'_{\text{odd}}(-\omega^2)\omega^3 + \sigma D'_{\text{even}}(-\omega^2)N'_{\text{odd}}(-\omega^2)\omega + N'_{\text{even}}(-\omega^2)(D'_{\text{even}}(-\omega^2) \\
& - \sigma D'_{\text{odd}}(-\omega^2))\omega, \\
q_2(\omega, \sigma) =& \omega \left[\{N'_{\text{odd}}(-\omega^2)\}^2\omega^2 + \{N'_{\text{even}}(-\omega^2)\}^2\right].
\end{aligned}$$

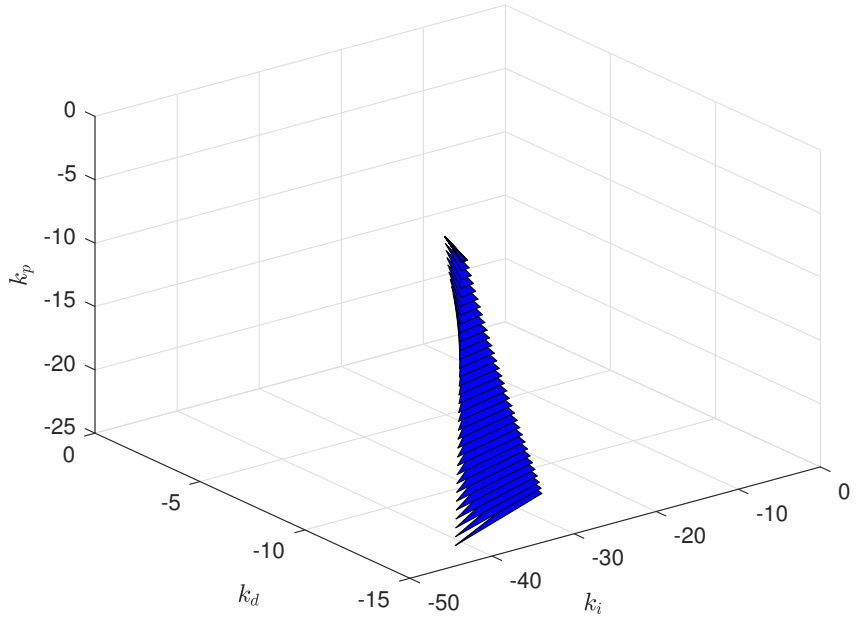

Figure 4.6: $\mathcal{S}(\sigma)$ set for $\sigma = 0.1$. © 2018 IEEE

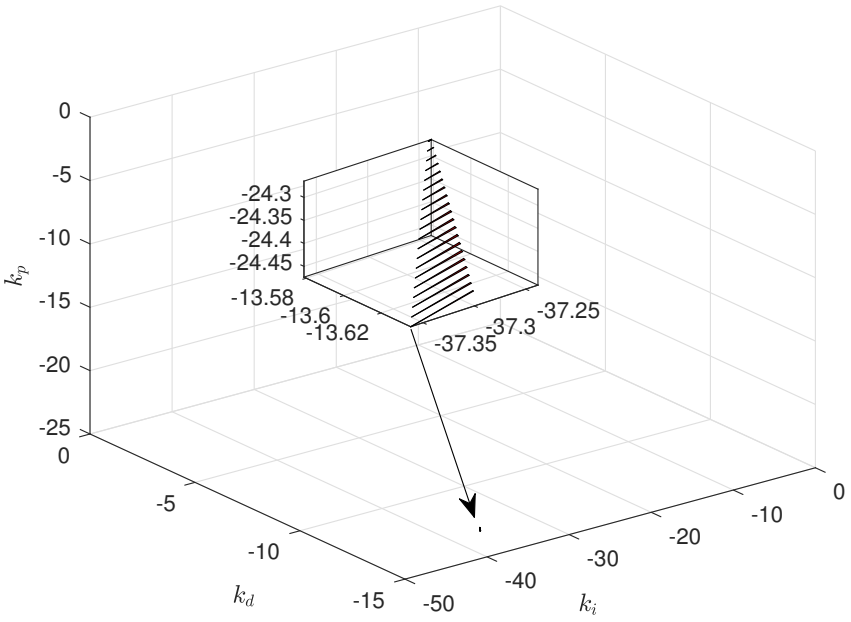

Figure 4.7: $\mathcal{S}(\sigma)$ set for $\sigma = 0.1655$. © 2018 IEEE

The sets $\mathcal{S}(\sigma)$ are displayed in Fig. 4.5, Fig. 4.6 and Fig. 4.7. The maximum achievable σ is found to be 0.1655. The algorithm allows us to observe how these sets shrink in a telescoping manner as σ increases. Of course, the complexity of computation of the stabilizing sets increases with the order of the system because the number of linear inequalities increases.

Example 4.8. Current control of AC drives Three-phase dynamic systems can be modeled as complex transfer functions. (See [27], [28] and [29] for details.) The complex transfer function representation assumes that the input and output signals are also of a complex form. For current control, in particular, the surface-mounted permanent-magnet synchronous machine is modeled by a first order complex transfer function and the tracking PI controller is tuned to cancel the plant pole which is stable. See Fig. 9 in [27] and Fig. 2 (b) in [29] for more details.

In a unity feedback control loop, the plant and the controller in the rotating dq frame can be represented in Fig. 4.8, where ω_e is the synchronous frequency, L and R are stator inductance and resistance, T_d the computation and modulation time delay, k a design parameter of the controller.

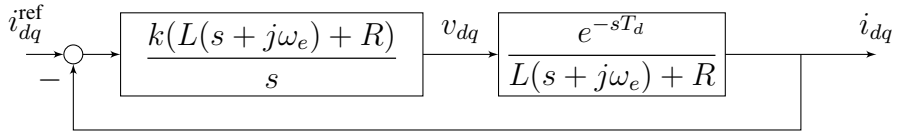

Figure 4.8: Block diagram for a surface-mounted permanent-magnet synchronous machine: i_{dq}^{ref} is the reference current, i_{dq} is the current output, v_{dq} is the voltage, all are in the rotating dq frame.

Specific values for ω_e, L, R and T_d were taken from [29].

We replaced the delay term e^{-sT_d} with the second-order Padé approximation. Then, the resulting closed loop system is the same as in Fig. 2.5 where

$$C(s) = \frac{k}{s}, \quad P(s) = \frac{1 - \frac{1}{2}T_d s + \frac{1}{12}T_d^2 s^2}{1 + \frac{1}{2}T_d s + \frac{1}{12}T_d^2 s^2}. \tag{4.42}$$

Setting $k_p = 0$, $k_i = k$ and $k_d = 0$ in (4.6), we have

$$\begin{aligned}
\delta'(s') &= (s' - \sigma)\left(\frac{1}{12}T_d^2(s' - \sigma)^2 + \frac{1}{2}T_d(s' - \sigma) + 1\right) \\
&\quad + k\left(\frac{1}{12}T_d^2(s' - \sigma)^2 - \frac{1}{2}T_d(s' - \sigma) + 1\right) \\
N'(-s') &= \frac{1}{12}T_d^2(s' + \sigma)^2 + \frac{1}{2}T_d(s' + \sigma) + 1
\end{aligned}$$

and

$$\begin{aligned}
\nu'(s') &= \delta'(s')N'(-s') \\
\nu'(j\omega) &= p_1(\omega, \sigma, T_d) + kp_2(\omega, \sigma, T_d) + jq(\omega, \sigma, T_d)
\end{aligned}$$

where

$$
\begin{aligned}
p_1(\omega,\sigma,T_d) &= -\frac{1}{12}\left(\frac{1}{12}\sigma T_d^4 - T_d^3\right)\omega^4 \\
&\quad -\left(\frac{1}{72}T_d^4\sigma^3 - \frac{1}{12}T_d^3\sigma^2 - \frac{5}{12}T_d^2\sigma + T_d\right)\omega^2 \\
&\quad -\frac{1}{144}T_d^4\sigma^5 + \frac{1}{12}T_d^2\sigma^3 - \sigma, \\
p_2(\omega,\sigma,T_d) &= \frac{1}{144}T_d^4\omega^4 + \frac{1}{12}\left(\frac{1}{6}T_d^4\sigma^2 + T_d^3\sigma + T_d^2\right)\omega^2 \\
&\quad +\frac{1}{144}T_d^4\sigma^4 + \frac{1}{12}T_d^3\sigma^3 + \frac{5}{12}T_d^2\sigma^2 + T_d\sigma + 1,
\end{aligned}
$$

$$
\begin{aligned}
q(\omega,\sigma,T_d) &= \frac{1}{144}T_d^4\omega^5 + \frac{1}{12}\left(\frac{1}{6}T_d^4\sigma^2 + T_d^3\sigma - 5T_d^2\right)\omega^3 \\
&\quad +\frac{1}{12}\left(\frac{1}{12}T_d^4\sigma^4 + T_d^3\sigma^3 - T_d^2\sigma^2\right)\omega - (T_d\sigma - 1)\,\omega.
\end{aligned}
$$

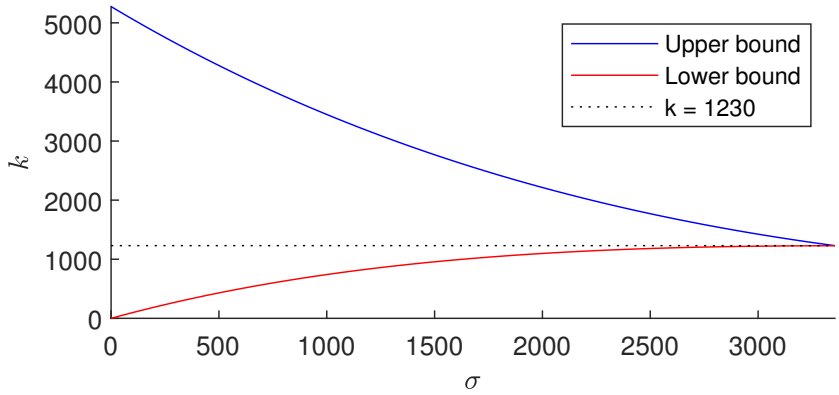

Figure 4.9: Stabilizing k bounds vs. σ. © 2018 IEEE

The sets $S(\sigma)$ are intervals in k axis and the upper and lower bounds for each interval with a prescribed σ are plotted in Fig. 4.9. $S(\sigma)$ just becomes empty at around $\sigma = 3356$ and the corresponding k is around 1230. Both values match the experimental result of [29] for the sampling frequency f_s of 5 kHz.

4.5 Notes and References

In [30], a linear quadratic regulator (LQR) design with a prescribed stability degree was proposed using state feedback. The control law minimized a quadratic performance index and the closed-loop poles had real part less than $-\sigma$. In [31], a branch and bound algorithm for computing the stability degree was proposed when the system was subject to parametric perturbations. A state feedback controller design with a prescribed damping ratio as well as the stability degree was proposed in [32]. The algorithm was based on the control law by which the closed loop poles were inside a prescribed disk.

A procedure for calculating PID gains for 'optimal' stability degree was proposed in [33]. The plant model was assumed to be all-pole, that is, the plant had no zeros.

In dominant pole placement, the design objective is to find a controller that places a pair of closed loop poles at the desired locations. A PID controller design approach was proposed in [34, 35], first-order controller in [36] and Proportional-Integral-Retarded (PIR) controller in [37]. After the controller gains were obtained, stability of the closed loop had to be checked and the locations of the rest of the closed loop poles had to be to the left of the pair of so-called 'dominant' poles.

5. DYNAMIC COMPENSATOR DESIGN USING LQR METHOD

Kalman's Linear Quadratic Regulator finds the optimal control law that minimizes a quadratic performance index for a given system. The control law is then implemented by an observer and the design of observer dynamics is decoupled from that of the optimal control law. We introduce an optimal control design method that contains the compensator dynamics at the outset by augmenting the original plant dynamics with a series of ingetrators. The quadratic performance index for the augmented system is minimized by an optimal control law and we exploit the control law to construct the compensator dynamics. A design parameter ρ is introduced and we show by numerical examples that a multi-objective design can be carried out by sweeping over the parameter values for which the stability of the feedback closed loop system is guaranteed.

5.1 Introduction

The plant dynamics is represented by

$$\dot{x}(t) = Ax(t) + Bu(t)$$

where (A, B) is controllable. The objective of control is to minimize the quadratic performance index:

$$\mathcal{I} = \int_0^\infty x'(t)Qx(t) + u'(t)Ru(t)dt$$

where $Q = Q' \geq 0$ and $R = R' > 0$. The control law is of form:

$$u(t) = -Kx(t)$$

and

$$K = R^{-1}B'P$$

where P is a solution of the algebraic Riccati equation:

$$A'P + PA + Q - PBR^{-1}B'P = 0.$$

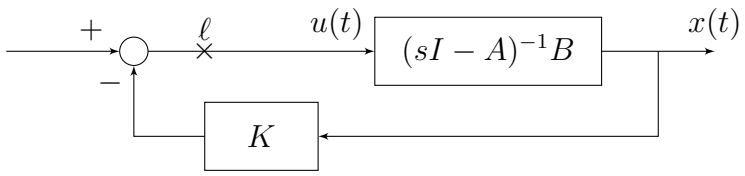

Figure 5.1: State feedback loop. ℓ is the loop breaking point.

The state feedback loop, as shown in Fig. 5.1, has the loop transfer function $L_1(s)$

$$L_1(s) = K(sI - A)^{-1}B.$$

It can be shown from Kalman's Return Difference relation [3] that the minimum stability margins of the system in Fig. 5.1 at the breaking point ℓ are

$$\text{Gain Margin: } \left[\frac{1}{2},\ \infty\right]$$

$$\text{Phase Margin: } (-60^o,\ 60^o)$$

If all the states are not directly measured, their estimates $\hat{x}(t)$ are generated by an observer:

$$\dot{\hat{x}} = A\hat{x} + Bu(t) + L(y(t) - C\hat{x}(t))$$

$$u(t) = -K\hat{x}$$

From the block diagram corresponding to the observer shown in Fig. 5.2 the loop transfer

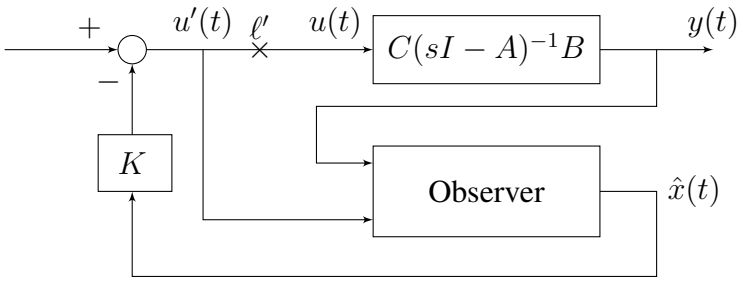

Figure 5.2: Observer-based output feedback loop. ℓ' is the loop breaking point.

function at the loop breaking point ℓ' can be calculated.

$$
\begin{aligned}
y(s) &= C(sI - A)^{-1}Bu \\
\hat{x}(s) &= (sI - A + LC)^{-1}Bu'(s) + (sI - A + LC)^{-1}Ly(s) \\
u'(s) &= -K\hat{x}(s).
\end{aligned}
$$

Let

$$
\begin{aligned}
R_1(s) &:= (sI - A + LC)^{-1} \\
R_2(s) &:= (sI - A + LC)^{-1}LC(sI - A)^{-1}.
\end{aligned}
$$

Then the loop transfer function $L_2(s)$ is

$$
L_2(s) = (I + KR_1(s)B)^{-1}KR_2(s)B.
$$

It is clear that $L_2(s)$ deviates from $L_1(s)$. Thus, the minimum stability margins of $L_1(s)$ could not be attained by using observers. Now, we revisit the example by Doyle and Stein [38].

Example 5.1. Consider the plant:

$$
\dot{x} = \begin{bmatrix} 0 & 1 \\ -3 & -4 \end{bmatrix} x + \begin{bmatrix} 0 \\ 1 \end{bmatrix} u
$$

$$y = \begin{bmatrix} 2 & 1 \end{bmatrix} x$$

and controller:

$$u = \begin{bmatrix} -50 & -10 \end{bmatrix} \hat{x} + \begin{bmatrix} 50 \end{bmatrix} r$$

where $\hat{x}$ is the estimated variable of x. The controller is linear quadratic optimal, corresponding to the performance index

$$\mathcal{I} = \int_0^\infty \left(x^T H^T H x + u^2 \right) dt$$

with

$$H = 4\sqrt{5} \begin{bmatrix} \sqrt{35} & 1 \end{bmatrix}.$$

It places the closed loop poles at

$$-7.0 \pm j\, 2.0.$$

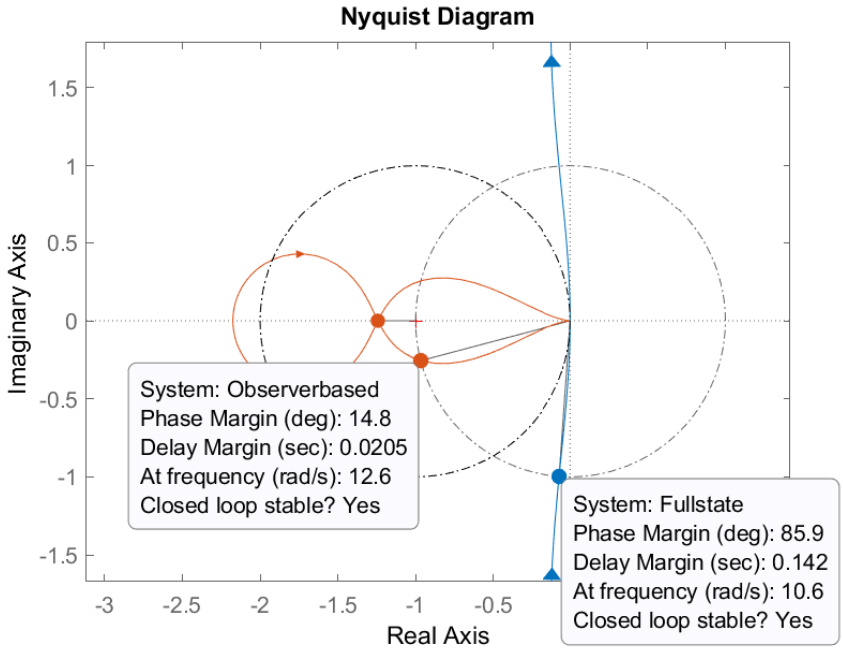

Figure 5.3: Nyquist plot for $L_1(s)$ (blue) and $L_2(s)$ (red).

Although the Kalman's LQR provides the phase margin of 86^o with state feedback, the implemented system with an observer-based compensator achieves less then 15^o.

We have made several observations in the following. The observer based compensator may not inherit Kalman's guaranteed stability margins. LQR problem is solved for n-th order plant but the overall closed loop system with compensators is of order (up to) $2n$. The loop breaking point for the state feedback case does not possess same physical meaning as that of output feedback. The phase margin of 15^o is somewhat surprising because the plant is stable and minimum-phase. The parameters were chosen particularly to make the resulting system look worse than how it would normally be.

Thus, we suggest that the order of the system that is optimized is same as the order of the system that is implemented. Moreover, we verify that the location of the closed loop poles is identical in both cases. In the following sections, following Pearson's original work and Bhattacharyya's extension using LQR method, we present the Dynamic Compensator design method where the observer is not used. In the design method, we employ a design parameter ρ and we are concerned with how much margins could be 'recovered' by varying the parameter ρ.

5.2 Optimal Dynamic Compensator

Consider a controllable and observable plant of order n,

$$\dot{x}(t) = Ax(t) + Bu(t) \tag{5.1}$$

with measurements

$$y(t) = Cx(t) \tag{5.2}$$

where $A \in \mathbb{R}^{n\times n}$, $B \in \mathbb{R}^{n\times r}$, $C \in \mathbb{R}^{m\times n}$ with $m < n$.

Let q be the smallest integer such that

$$\text{Rank} \begin{bmatrix} C \\ CA \\ \vdots \\ CA^q \end{bmatrix} = n. \tag{5.3}$$

Define

$$\begin{aligned} u_1(t) &:= \dot{u}(t), \\ u_2(t) &:= \dot{u}_1(t), \\ &\vdots \\ u_{q-1}(t) &:= \dot{u}_{q-2}(t), \\ v(t) &:= \dot{u}_{q-1}(t) \end{aligned}$$

This is a string of rq integrators.

Define

$$x_a(t) := \begin{bmatrix} x(t) \\ u(t) \\ u_1(t) \\ \vdots \\ u_{q-1}(t) \end{bmatrix}, \quad A_a := \begin{bmatrix} A & B & 0 & \cdots & 0 \\ 0 & 0 & I & \cdots & 0 \\ \vdots & \vdots & & \ddots & 0 \\ 0 & 0 & 0 & \cdots & I \\ 0 & 0 & 0 & \cdots & 0 \end{bmatrix}, \quad B_a := \begin{bmatrix} x(t) \\ u(t) \\ u_1(t) \\ \vdots \\ u_{q-1}(t) \end{bmatrix}$$

We have a state equation with $v(t)$ as an r-vector input.

$$\dot{x}_a(t) = A_a x(t) + B_a v(t) \tag{5.4}$$

The performance index is

$$J_a = \int_0^\infty x_a'(t)\, Q_a\, x_a(t) + v'(t)\, R_a\, v(t)\, dt \tag{5.5}$$

where $R_a = R_a' > 0$ and $Q_a = Q_a' \geq 0$ with (Q_a, A_a) observable.

The optimal control law is

$$\begin{aligned} v(t) &= -K_a x_a(t) \\ &= -\left(K_0 x(t) + L_0 u_(t) + \cdots + L_{q-1} u_{q-1}(t)\right) \end{aligned}$$

Since the observability matrix is of full rank, there exists a matrix $\begin{bmatrix} P_0 & P_1 & \cdots & P_q \end{bmatrix}$ such that

$$\begin{bmatrix} P_0 & P_1 & \cdots & P_q \end{bmatrix} \begin{bmatrix} C \\ CA \\ \vdots \\ CA^q \end{bmatrix} = K_0 \tag{5.6}$$

Observe that

$$\begin{aligned} y(t) &= Cx(t) \\ \dot{y}(t) &= CAx(t) + CBu(t) \\ &\vdots \\ y^{(q)}(t) &= CA^q x(t) + CA^{q-1}Bu(t) + CA^{q-2}Bu_1(t) + \cdots CBu_{q-1}(t) \end{aligned}$$

and that

$$\begin{aligned} K_0 x(t) =& P_0 Cx(t) + P_1 CAx(t) + \cdots + P_q CA^q x(t) \\ =& P_0 y(t) + P_1 \left(\dot{y}(t) - CBu(t)\right) + \cdots \end{aligned}$$

$$+ P_q \left(y^{(q)}(t) - CA^{q-1}Bu(t) - CA^{q-2}Bu_1(t) - \cdots CBu_{q-1}(t) \right).$$

Define

$$\begin{aligned} Q_0 &:= L_0 - P_1CB - P_2CAB - \cdots - P_qCA^{q-1}B \\ Q_1 &:= L_1 - P_2CB - P_3CAB - \cdots - P_qCA^{q-2}B \\ &\vdots \\ Q_{q-1} &:= L_{q-1} - P_qCB. \end{aligned}$$

Since

$$v(t) = \dot{u}_{q-1}(t) = \frac{d^q u(t)}{dt^q},$$

we obtain

$$\frac{d^q u(t)}{dt^q} + Q_{q-1}\frac{d^{q-1}u(t)}{dt^{q-1}} + \cdots + Q_0 u(t) = -P_q\frac{d^q y(t)}{dt^q} - P_{q-1}\frac{d^{q-1}y(t)}{dt^{q-1}} - \cdots - P_0 y(t).$$

Define

$$\begin{aligned} Q(s) &:= s^q I + s^{q-1}Q_{q-1} + \cdots + Q_0 \\ P(s) &:= P_q s^q + P_{q-1}s^{q-1} + \cdots + P_0 \end{aligned}$$

We obtain

$$u(s) = Q^{-1}(s)P(s)(-y(s)). \tag{5.7}$$

Or alternatively,

$$-u(s) = Q^{-1}(s)P(s)y(s). \tag{5.8}$$

The compensator has the following state variable equations:

$$\begin{bmatrix} \dot{z}_1(t) \\ \dot{z}_2(t) \\ \vdots \\ \dot{z}_q(t) \end{bmatrix} = \underbrace{\begin{bmatrix} 0 & \cdots & 0 & -Q_0 \\ I & \cdots & 0 & -Q_1 \\ 0 & \ddots & 0 & \vdots \\ 0 & \cdots & I & -Q_{q-1} \end{bmatrix}}_{=:A_c} \begin{bmatrix} z_1(t) \\ z_2(t) \\ \vdots \\ z_q(t) \end{bmatrix} + \underbrace{\begin{bmatrix} P_0 - Q_0 P_q \\ P_1 - Q_1 P_q \\ \vdots \\ P_{q-1} - Q_{q-1} P_q \end{bmatrix}}_{=:B_c} y(t)$$

$$-u(t) = \underbrace{\begin{bmatrix} 0 & \cdots & 0 & I \end{bmatrix}}_{=:C_c} \begin{bmatrix} z_1(t) \\ z_2(t) \\ \vdots \\ z_q(t) \end{bmatrix} + \underbrace{P_q}_{=:D_c} y(t)$$

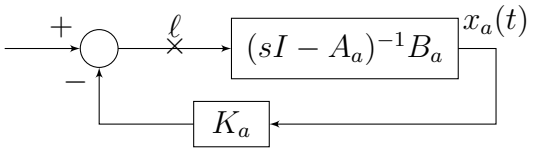

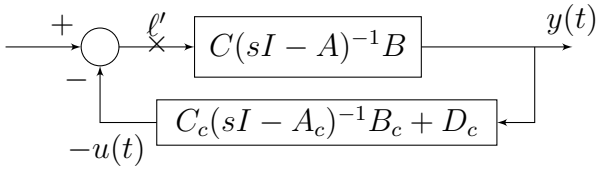

Figure 5.4: Block diagrams for the augmented system (top) and for the closed loop with dynamic compensator (bottom).

The closed loop dynamics is

$$\begin{aligned} \dot{x} &= Ax + Bu \\ &= Ax - B(-u) \\ &= Ax - B(C_c z + D_c y) \end{aligned}$$

$$= (A - BD_cC)x - BC_cz$$

$$\dot{z} = A_cz + B_cy$$

$$= B_cCx + A_cz$$

so that

$$A_{cl} = \begin{bmatrix} A - BD_cC & -BC_c \\ B_cC & A_c \end{bmatrix}.$$

Lemma 5.2. *$A_a - B_aK_a$ and A_{cl} are similar.*

Proof. Let

$$T := \begin{bmatrix} A^q & A^{q-1}B & \cdots & AB & B \\ P_0CA^{q-1} & P_0CA^{q-2}B & \cdots & P_0CB & Q_0 \\ \vdots & \vdots & \ddots & \vdots & \vdots \\ \sum_{i=0}^{q-2} P_iCA^{i+1} & \sum_{i=0}^{q-2} P_iCA^iB & \cdots & P_{q-2}CB + Q_{q-3} & Q_{q-2} \\ \sum_{i=0}^{q-1} P_iCA^i & \sum_{i=1}^{q-1} P_iCA^{i-1}B + Q_0 & \cdots & P_{q-1}CB + Q_{q-2} & Q_{q-1} \end{bmatrix}.$$

Then,

$$T(A_a - B_aK_a) = A_{cl}T.$$

□

Example 5.3. Doyle and Stein's Example

Let

$$Q_a = \begin{bmatrix} 2800 & 80\sqrt{35} & 0 \\ 80\sqrt{35} & 80 & 0 \\ 0 & 0 & 1 \end{bmatrix}, \quad R_a = \rho I.$$

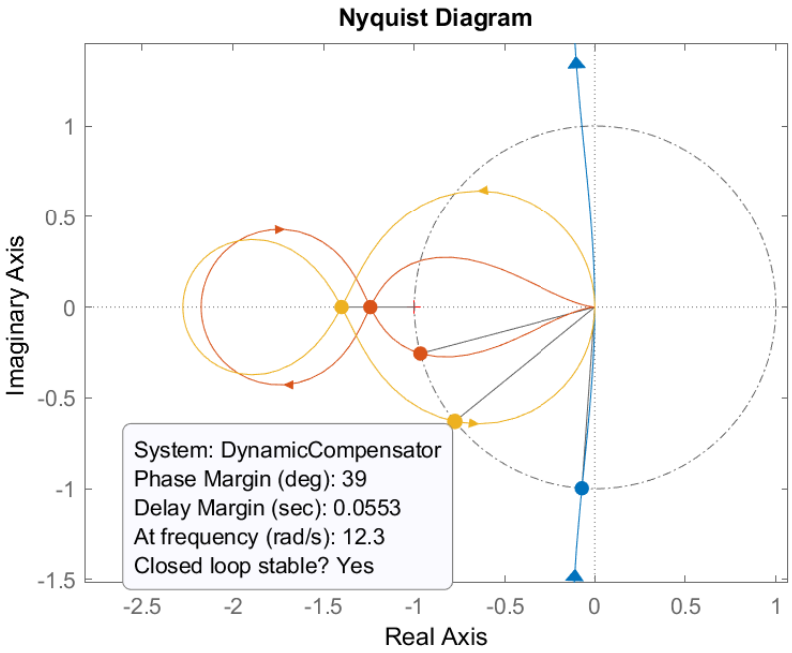

Figure 5.5: Nyquist plot with $\rho = 1$.

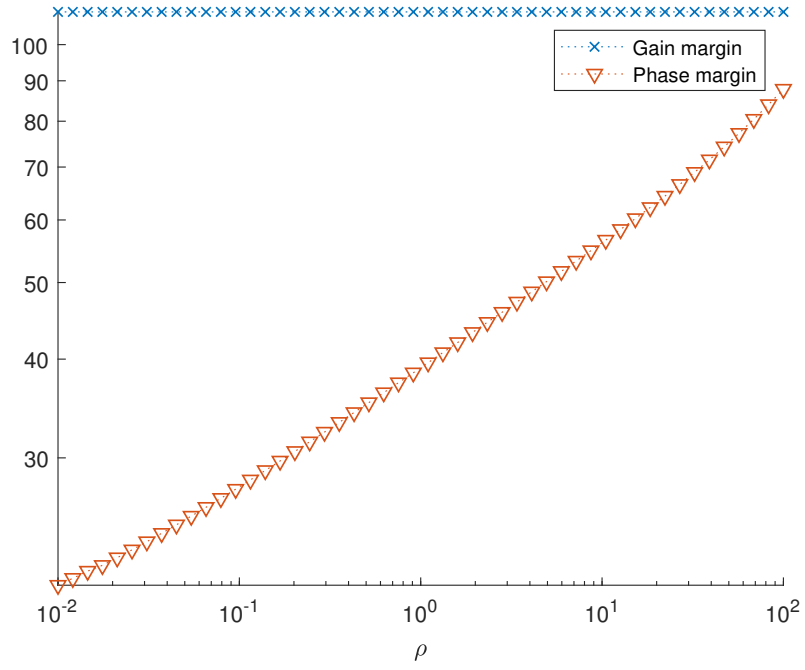

Figure 5.6: Gain and Phase margins versus $\rho \in (0.01, 100)$

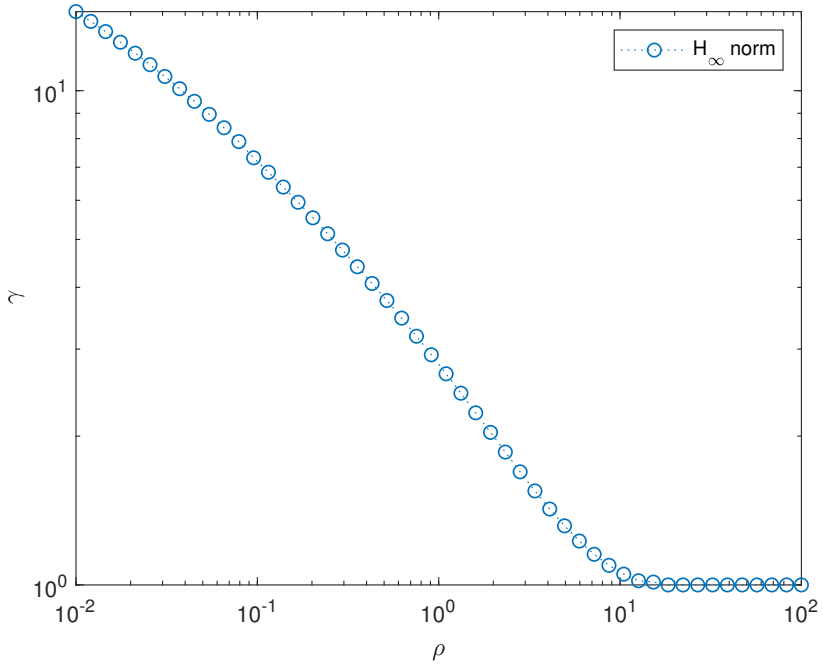

Figure 5.7: H_∞ norm versus $\rho \in (0.01, 100)$

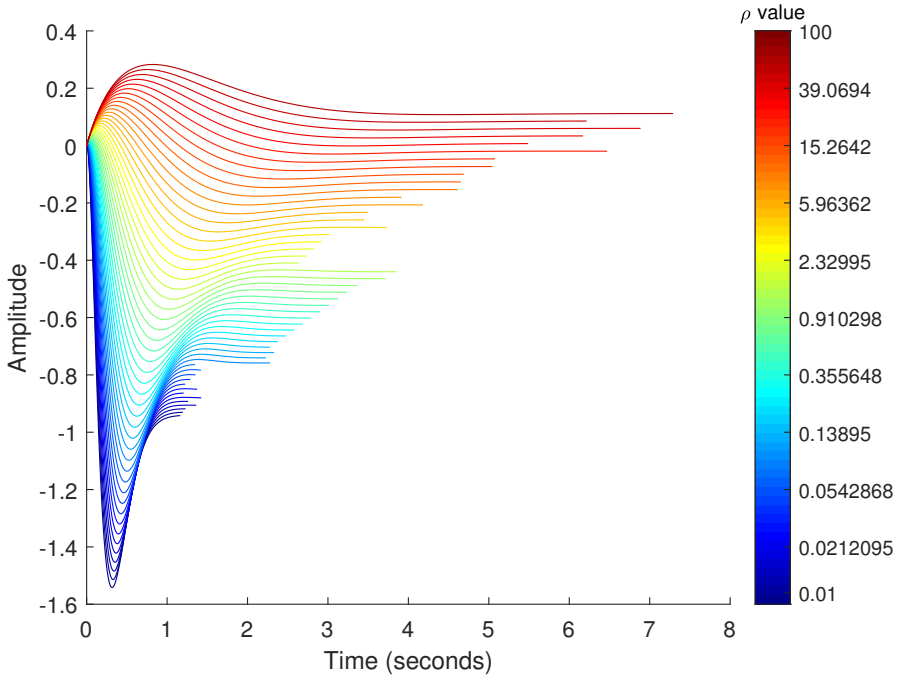

Figure 5.8: Step reseponses for $\rho \in (0.01, 100)$

If we choose a $\rho \in (0.01, 100)$, we have a corresponding controller. Since this is a regulator design problem, the step responses have nonzero steady state errors. In the following section, we consider the LQR problem to design a servo controller.

5.3 Servomechanism Compensator Design

We add a bank of integrators and define a 'New Plant'.

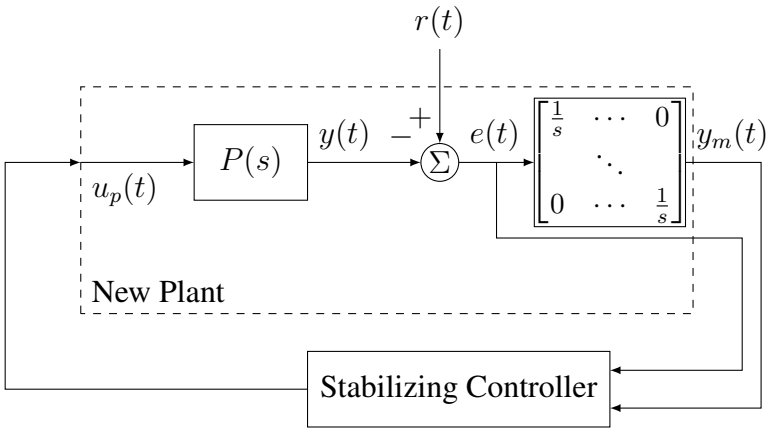

Figure 5.9: Stabilizing Controller

Input to the new plant is $u_p(t)$ and output is $e(t)$ and $y_m(t)$. Let $r(t) \equiv 0$.

$$\begin{bmatrix} \dot{x}_p(t) \\ \dot{x}_m(t) \end{bmatrix} = \underbrace{\begin{bmatrix} A_p & 0 \\ -B_m C_p & A_m \end{bmatrix}}_{A} \begin{bmatrix} x_p(t) \\ x_m(t) \end{bmatrix} + \underbrace{\begin{bmatrix} B_p \\ -B_m D_p \end{bmatrix}}_{B} u_p(t)$$

$$\begin{bmatrix} e(t) \\ y_m(t) \end{bmatrix} = \begin{bmatrix} -y_p(t) \\ y_m(t) \end{bmatrix} = \underbrace{\begin{bmatrix} -C_p & 0 \\ 0 & C_m \end{bmatrix}}_{C} \begin{bmatrix} x_p(t) \\ x_m(t) \end{bmatrix} \underbrace{-D_p}_{D} u_p(t).$$

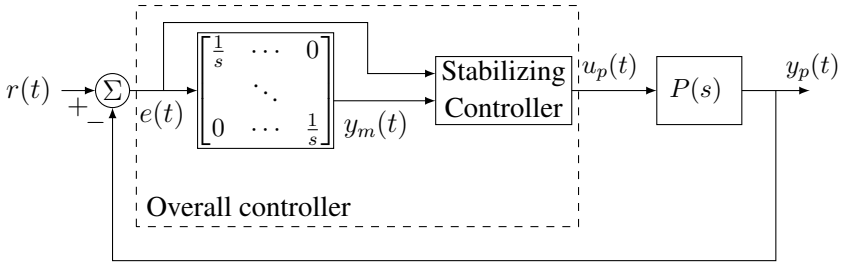

Figure 5.10: Unity feedback multivariable control loop

Example 5.4. We consider the same example and design a servo controller in Fig.5.10.

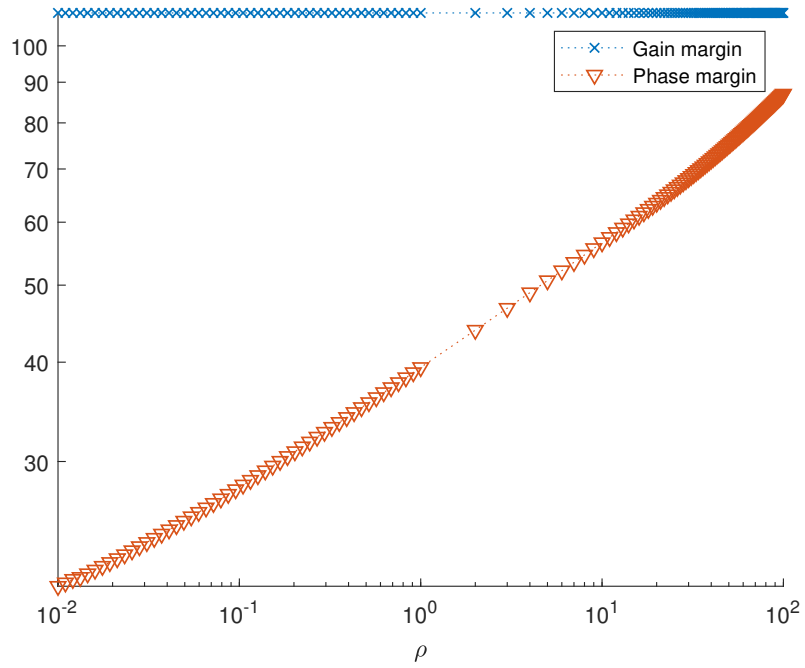

Figure 5.11: Gain and Phase margins versus $\rho \in (0.01, 100)$

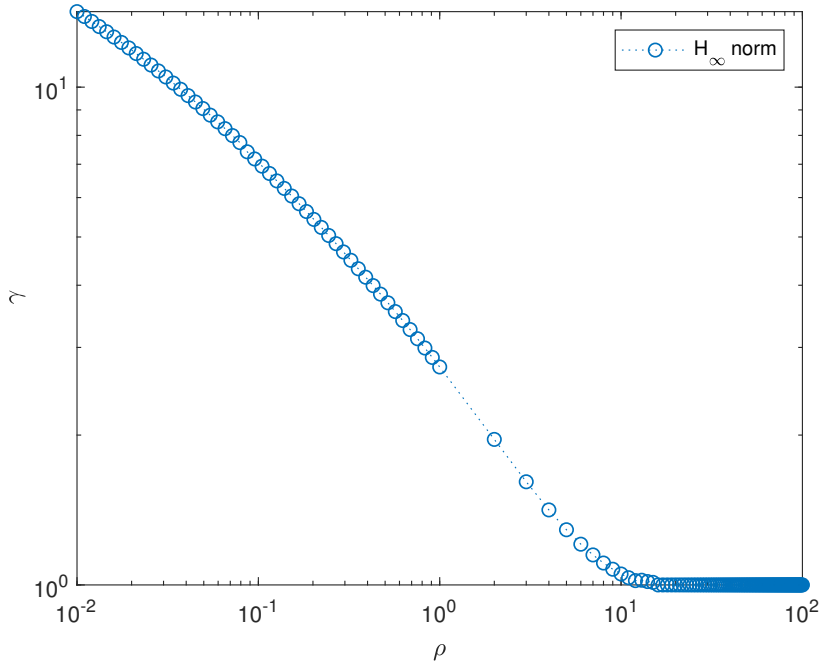

Figure 5.12: H_∞ norms versus $\rho \in (0.01, 100)$

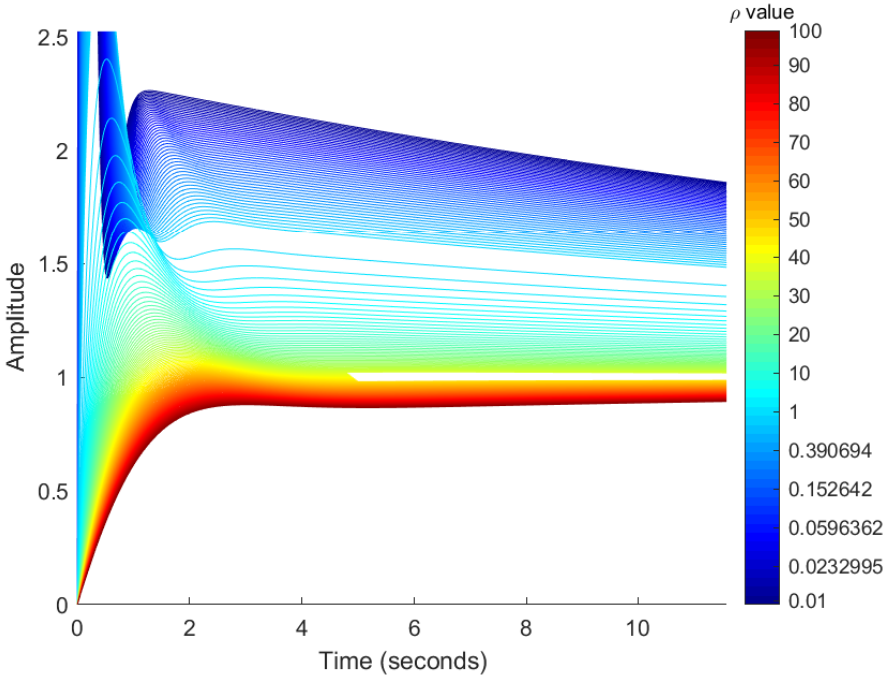

Figure 5.13: Step responses for $\rho \in (0.01, 100)$

For instance, we choose $\rho = 41$ as our design point.

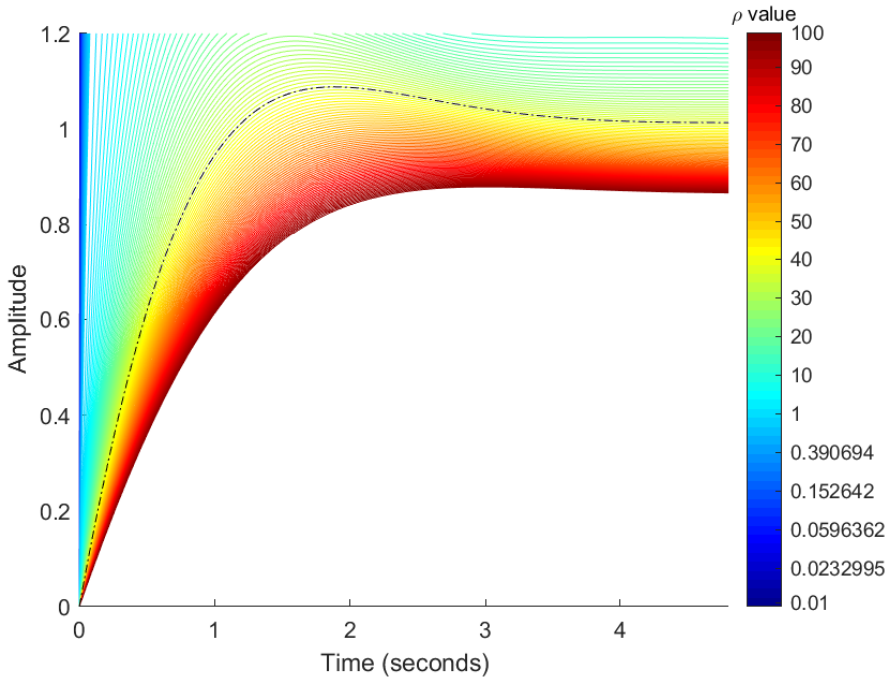

Figure 5.14: The step response for $\rho = 41$ (black dashed).

We can retrieve the controller:

$$C(s) = \frac{1.553s^2 + 4.275s + 0.1562}{s^2 - 0.01544s}$$

The closed loop poles are $-3.0987, -1.2004 \pm j1.1092, -0.0377$ which are same as the eigenvalues of $A_a - B_a K_a$. The control effort for $\rho = 41$ is shown in Fig. 5.15.

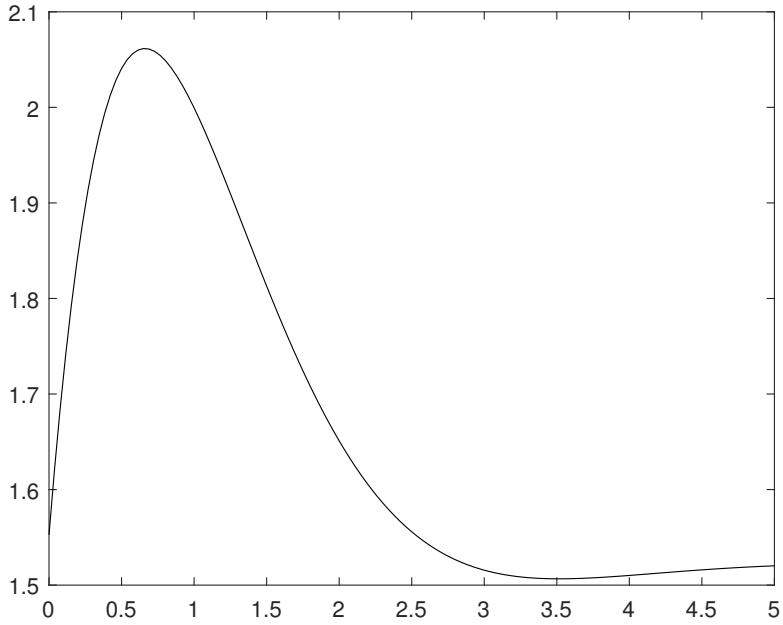

Figure 5.15: $u(t)$ for $\rho = 41$.

Example 5.5. Multivariable Example The plant is [39]:

$$Ap = \begin{bmatrix} -1 & 0 & 0 & 0 \\ 0 & -1 & 0 & 0 \\ 0 & 0 & -0.2 & 0 \\ 0 & 0 & 0 & -0.2 \end{bmatrix}, \; Bp = \begin{bmatrix} -0.5 & 1.25 \\ -2.5 & -2.5 \\ 0.3 & -1.25 \\ 1.5, 3.5 & \end{bmatrix}$$

$$Cp = \begin{bmatrix} 1 & 0 & 1 & 0 \\ 0 & 1 & 0 & 1 \end{bmatrix}$$

In Fig. 5.16, the step responses for the observer based controller are shown. In Figs. 5.17, 5.18, 5.19 and 5.20, the step responses for the optimal dynamic compensator with varying ρ are shown.

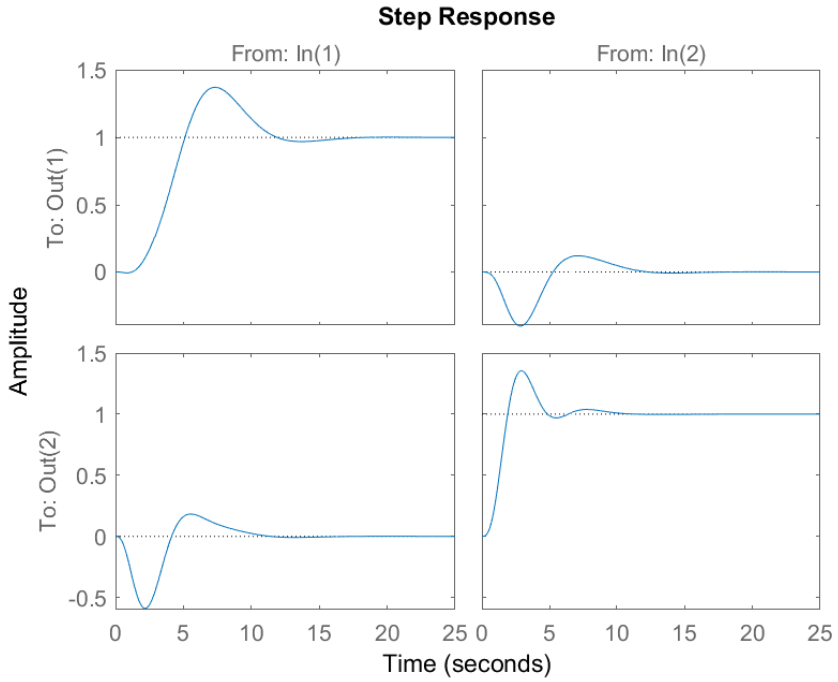

Figure 5.16: Multivariable Step responses for the observer based controller.

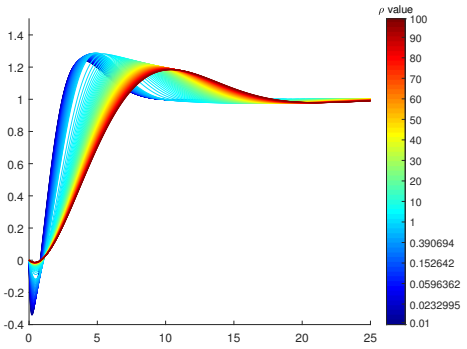

Figure 5.17: Input 1 to Output 1

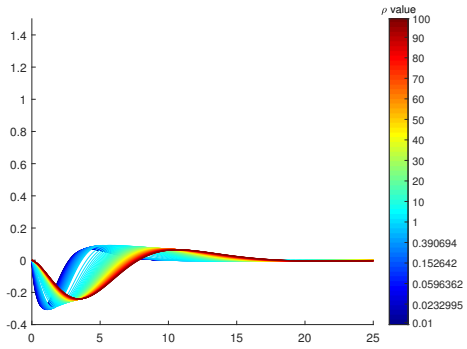

Figure 5.18: Input 2 to Output 1

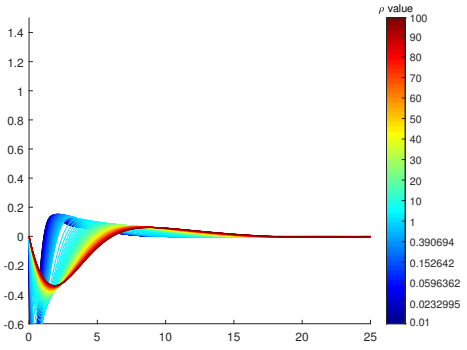

Figure 5.19: Input 1 to Output 2

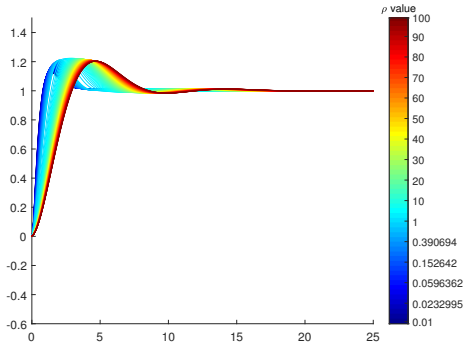

Figure 5.20: Input 2 to Output 2

6. SUMMARY

We presented systematic and constructive determination of subsets of the stabilizing set $\mathcal{S}$ of PI and PID controllers for Linear Time Invariant systems. Having the stabilizing set at the outset, we expressed the design criteria in terms of controller parameters; superimposed over the stabilizing set to get the subset satisfying design criteria; obtain the maximum achievable performance by pushing the criteria until the subset just becomes empty.

The H_∞ criterion provides the robustness of the closed loop in terms of the H_∞ norm of the error transfer function while the σ-Hurwitz stability provides time domain optimality of the closed loop. As a result, we can have a way to construct a systematic methodology in which we find the subset of PID controllers that achieve multiple design objectives efficiently and analytically.

Time domain controller synthesis exploiting the stabilizing set $\mathcal{S}$ and achievable performance curves indexed by design parameters in the controller parameter space is a good area of future research.

Optimal dynamic compensator for pole placement was first introduced by Pearson in 1969 [40]. Brasch, Pearson and Ding extended it to multivariable systems [41, 42], respectively. Bhattacharyya applied the Dynamic Compensator concept using LQR method in [3]. We gave an approach where we have a simple design parameter. We also considered a servomechanism case which must be the ultimate objective of any control system design.

Extend the LQR method to the so-called Brasch-Pearson compensators [41] is also a good research problem.

REFERENCES

[1] A. Datta, M.-T. Ho, and S. P. Bhattacharyya, *Structure and synthesis of PID controllers*. Springer Science & Business Media, 2013.

[2] G. J. Silva, A. Datta, and S. P. Bhattacharyya, *PID controllers for time-delay systems*. Springer Science & Business Media, 2007.

[3] S. P. Bhattacharyya, A. Datta, and L. H. Keel, *Linear control theory: structure, robustness, and optimization*, vol. 33. CRC press, 2009.

[4] S. Han, L. H. Keel, and S. P. Bhattacharyya, "PID controller design with an H_∞ criterion," *IFAC-PapersOnLine*, vol. 51, no. 4, pp. 400 – 405, 2018. 3rd IFAC Conference on Advances in Proportional-Integral-Derivative Control PID 2018.

[5] T. Emami and J. M. Watkins, "Robust performance characterization of PID controllers in the frequency domain," *WSEAS transactions on systems and control*, vol. 4, no. 5, pp. 232–242, 2009.

[6] R. N. Tantaris, L. H. Keel, and S. P. Bhattacharyya, "H_∞ design with first-order controllers," *IEEE Transactions on Automatic Control*, vol. 51, no. 8, pp. 1343–1347, 2006.

[7] W. Krajewski and U. Viaro, "On robust PID control for time-delay plants," in *Methods and Models in Automation and Robotics (MMAR), 2012 17th International Conference on*, pp. 540–545, IEEE, 2012.

[8] B. S. Ashfaque and K. Tsakalis, "Discrete-Time PID Controller Tuning Using Frequency Loop-Shaping," *IFAC Proceedings Volumes*, vol. 45, no. 3, pp. 613–618, 2012.

[9] K. S. Tsakalis and S. Dash, "Approximate H_∞ loop shaping in PID parameter adaptation," *International Journal of Adaptive Control and Signal Processing*, vol. 27, no. 1-2, pp. 136–152, 2013.

[10] M. Tomizuka and S. Zhang, "Modelling and Conventional/Adaptive PI Control of a Lathe Cutting Process," in *1985 American Control Conference*, pp. 745–750, June 1985.

[11] M.-T. Ho, "Synthesis of H_∞ PID controllers: A parametric approach," *Automatica*, vol. 39, no. 6, pp. 1069–1075, 2003.

[12] E. N. Gryazina, B. T. Polyak, and A. A. Tremba, "Design of the low-order controllers by the H_∞ criterion: A parametric approach," *Automation and Remote Control*, vol. 68, no. 3, pp. 456–466, 2007.

[13] R. Joshi, *Process Control Applications in Microbial Fuel Cells (MFC)*. PhD thesis, Arizona State University, 2018.

[14] P. S. Malik, S. S. Gawas, I. AltafPatel, N. P. Parsekar, A. A. Parab, and S. S. Parkar, "Transient Response Improvement of DC to DC Converter by Using Auto-tuned PID Controller," in *2018 Second International Conference on Inventive Communication and Computational Technologies (ICICCT)*, pp. 546–549, IEEE, 2018.

[15] R. Hernández-Alvarado, L. García-Valdovinos, T. Salgado-Jiménez, A. Gómez-Espinosa, and F. Fonseca-Navarro, "Neural network-based self-tuning PID control for underwater vehicles," *Sensors*, vol. 16, no. 9, p. 1429, 2016.

[16] E. Abbasi and N. Naghavi, "Offline Auto-Tuning of a PID Controller Using Extended Classifier System (XCS) Algorithm," *Journal of Advances in Computer Engineering and Technology*, vol. 3, no. 1, pp. 41–44, 2017.

[17] S. Ganjefar and M. Alizadeh, "On-line self-learning PID based PSS using self-recurrent wavelet neural network identifier and chaotic optimization," *COMPEL-The international journal for computation and mathematics in electrical and electronic engineering*, vol. 31, no. 6, pp. 1872–1891, 2012.

[18] T.-H. Kim, I. Maruta, and T. Sugie, "Robust PID controller tuning based on the constrained particle swarm optimization," *Automatica*, vol. 44, no. 4, pp. 1104–1110, 2008.

[19] E. Dincel and M. T. Söylemez, "Digital PI-PD controller design for arbitrary order systems: Dominant pole placement approach," *ISA transactions*, vol. 79, pp. 189–201, 2018.

[20] H. Bevrani, T. Hiyama, and H. Bevrani, "Robust PID based power system stabiliser: Design and real-time implementation," *International Journal of Electrical Power & Energy Systems*, vol. 33, no. 2, pp. 179–188, 2011.

[21] S. K. Pandey, N. Kishor, and S. R. Mohanty, "Frequency regulation in hybrid power system using iterative proportional-integral-derivative H_∞ controller," *Electric Power Components and Systems*, vol. 42, no. 2, pp. 132–148, 2014.

[22] B. J. Patella, A. Prodic, A. Zirger, and D. Maksimovic, "High-frequency digital controller IC for DC/DC converters," in *APEC. Seventeenth Annual IEEE Applied Power Electronics Conference and Exposition (Cat. No. 02CH37335)*, vol. 1, pp. 374–380, IEEE, 2002.

[23] K. Sharma and D. K. Palwalia, "Design of digital PID controller for voltage mode control of DC-DC converters," in *2017 International conference on Microelectronic Devices, Circuits and Systems (ICMDCS)*, pp. 1–6, IEEE, 2017.

[24] T. Ariyachartphadungkit, R. Vanijjirattikhan, and S. Hasegawa, "Implementation of PID posture controller for 6 DOF underwater robot," in *2016 International Conference on Electronics, Information, and Communications (ICEIC)*, pp. 1–4, IEEE, 2016.

[25] A. Hamed, E. Shaban, R. Darwish, *et al.*, "Design and implementation of discrete PID control applied to Bitumen tank based on new approach of pole placement technique," *International Journal of Dynamics and Control*, vol. 5, no. 3, pp. 604–613, 2017.

[26] H. S. Khan and M. B. Kadri, "Attitude and altitude control of quadrotor by discrete PID control and non-linear model predictive control," in *2015 International Conference on Information and Communication Technologies (ICICT)*, pp. 1–11, IEEE, 2015.

[27] F. Briz, M. W. Degner, and R. D. Lorenz, "Analysis and design of current regulators using complex vectors," *IEEE Transactions on Industry Applications*, vol. 36, no. 3, pp. 817–825, 2000.

[28] L. Harnefors, "Modeling of three-phase dynamic systems using complex transfer functions and transfer matrices," *IEEE Transactions on Industrial Electronics*, vol. 54, no. 4, pp. 2239–2248, 2007.

[29] A. G. Yepes, A. Vidal, J. Malvar, O. López, and J. Doval-Gandoy, "Tuning method aimed at optimized settling time and overshoot for synchronous proportional-integral current control in electric machines," *IEEE Transactions on Power Electronics*, vol. 29, no. 6, pp. 3041–3054, 2014.

[30] B. D. Anderson and J. B. Moore, "Linear system optimisation with prescribed degree of stability," vol. 116, no. 12, pp. 2083–2087, 1969.

[31] V. Balakrishnan, S. Boyd, and S. Balemi, "Branch and bound algorithm for computing the minimum stability degree of parameter-dependent linear systems," *International Journal of Robust and Nonlinear Control*, vol. 1, no. 4, pp. 295–317, 1991.

[32] P. Misra, "LQR design with prescribed damping and degree of stability," in *Computer-Aided Control System Design, 1996., Proceedings of the 1996 IEEE International Symposium on*, pp. 68–70, IEEE, 1996.

[33] A. Shubladze, "A procedure for calculating the optimal stability of PID controls. 2.," *Automation and Remote Control*, vol. 48, no. 6, pp. 748–756, 1987.

[34] S. Srivastava and V. Pandit, "A PI/PID controller for time delay systems with desired closed loop time response and guaranteed gain and phase margins," *Journal of Process Control*, vol. 37, pp. 70–77, 2016.

[35] E. Dincel and M. T. Söylemez, "Limitations on dominant pole pair selection with continuous PI and PID controllers," in *Control, Decision and Information Technologies (CoDIT), 2016 International Conference on*, pp. 741–745, IEEE, 2016.

[36] A. Madady and H.-R. Reza-Alikhani, "First-order controllers design employing dominant pole placement," in *Control & Automation (MED), 2011 19th Mediterranean Conference on*, pp. 1498–1503, IEEE, 2011.

[37] A. Ramírez, S. Mondié, and R. Garrido, "Proportional integral retarded control of second order linear systems," in *Decision and Control (CDC), 2013 IEEE 52nd Annual Conference on*, pp. 2239–2244, IEEE, 2013.

[38] J. Doyle and G. Stein, "Robustness with observers," *IEEE transactions on automatic control*, vol. 24, no. 4, pp. 607–611, 1979.

[39] B. M. Chen, A. Saberi, and P. Sannuti, "Necessary and sufficient conditions for a nonminimum phase plant to have a recoverable target loopa stable compensator design for ltr," *Automatica*, vol. 28, no. 3, pp. 493–507, 1992.

[40] J. Pearson and C. Ding, "Compensator design for multivariable linear systems," *IEEE Transactions on Automatic Control*, vol. 14, no. 2, pp. 130–134, 1969.

[41] F. Brasch and J. Pearson, "Pole placement using dynamic compensators," *IEEE Transactions on Automatic Control*, vol. 15, no. 1, pp. 34–43, 1970.

[42] C. Ding, F. Brasch, and J. Pearson, "On multivariable linear systems," *IEEE Transactions on Automatic Control*, vol. 15, no. 1, pp. 96–97, 1970.